Accepted Manuscript

Structure-activity relationship of new antimalarial 1-aryl-3-susbtituted propanol derivatives: Synthesis, preliminary toxicity profiling, parasite life cycle stage studies, target exploration, and targeted delivery

Miguel Quiliano, Adriana Pabón, Ernest Moles, Leonardo Bonilla-Ramirez, Isabelle Fabing, Kim Y. Fong, Diego A. Nieto-Aco, David W. Wright, Juan C. Pizarro, Ariane Vettorazzi, Adela López de Cerain, Eric Deharo, Xavier Fernández-Busquets, Giovanny Garavito, Ignacio Aldana, Silvia Galiano

PII: S0223-5234(18)30372-6

DOI: 10.1016/j.ejmech.2018.04.038

Reference: EJMECH 10387

To appear in: *European Journal of Medicinal Chemistry*

Received Date: 18 February 2018

Revised Date: 16 April 2018

Accepted Date: 18 April 2018

Please cite this article as: M. Quiliano, A. Pabón, E. Moles, L. Bonilla-Ramirez, I. Fabing, K.Y. Fong, D.A. Nieto-Aco, D.W. Wright, J.C. Pizarro, A. Vettorazzi, A. López de Cerain, E. Deharo, X. Fernández-Busquets, G. Garavito, I. Aldana, S. Galiano, Structure-activity relationship of new antimalarial 1-aryl-3-susbtituted propanol derivatives: Synthesis, preliminary toxicity profiling, parasite life cycle stage studies, target exploration, and targeted delivery, *European Journal of Medicinal Chemistry* (2018), doi: 10.1016/j.ejmech.2018.04.038.

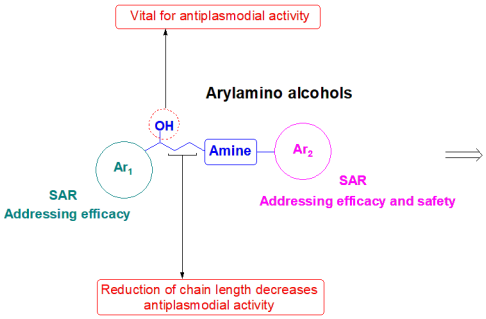

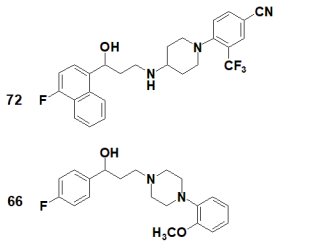

Antiplasmodial activity (3D7, D6, FCR-3, C235)
Antimalarial activity (*in vivo* parasitemia reduction)
High selectivity index and absence of genotoxicity
Multistage-activity profile (blood, liver, and mosquito)
Unknown primary mechanism of action

Structure-activity relationship of new antimalarial 1-aryl-3-susbtituted propanol derivatives: Synthesis, preliminary toxicity profiling, parasite life cycle stage studies, target exploration, and targeted delivery

Miguel Quiliano[a,b], *Adriana Pabón*[c], *Ernest Moles*[d,e,f], *Leonardo Bonilla-Ramirez*[c], *Isabelle Fabing*[g], *Kim Y. Fong*[h], *Diego A. Nieto-Aco*[a,b,1], *David W. Wright*[h], *Juan C. Pizarro*[i,j], *Ariane Vettorazzi*[k], *Adela López de Cerain*[k], *Eric Deharo*[l], *Xavier Fernández-Busquets*[d,e,f], *Giovanny Garavito*[m], *Ignacio Aldana* [a,b], *Silvia Galiano*[a,b] *(*)*

[a] Universidad de Navarra, Instituto de Salud Tropical (ISTUN), Campus Universitario, 31008 Pamplona, Spain

[b] Universidad de Navarra, Facultad de Farmacia y Nutrición, Departamento de Química Orgánica y Farmacéutica, Campus Universitario, 31008 Pamplona, Spain

[c] Grupo Malaria, Universidad de Antioquía, Medellín, Colombia

[d] Nanomalaria Group, Institute for Bioengineering of Catalonia (IBEC), Baldiri Reixac 10-12, 08028 Barcelona, Spain

[e] Barcelona Institute for Global Health (ISGlobal), Barcelona Center for International Health Research (CRESIB, Hospital Clínic-Universitat de Barcelona), Rosselló 149-153, 08036 Barcelona, Spain

[f] Nanoscience and Nanotechnology Institute (IN2UB), University of Barcelona, Martí i Franquès 1, 08028 Barcelona, Spain

[g] Laboratoire de Synthese et Physicochimie de Molécules d'Intéret Biologique SPCMIB-UMR5068, CNRS - Université Paul Sabatier, 118, route de Narbonne, 31062, Toulouse Cedex 09, France

[h] Department of Chemistry, Vanderbilt University, Station B 351822, Nashville, TN 37235, USA

[i] Department of Tropical Medicine, School of Public Health and Tropical Medicine, Tulane University

[j] Vector-Borne Infectious Diseases Research Center, Tulane University

[k] Universidad de Navarra, Facultad de Farmacia y Nutrición, Department of Pharmacology and Toxicology, Campus Universitario, 31008 Pamplona, Spain

[l] UMR 152 PHARMA-DEV, Université Toulouse, IRD, UPS, 31062, Toulouse, France

[m] Universidad Nacional de Colombia, Sede Bogotá, Facultad de Ciencias, Departamento de Farmacia (DFUNC), Grupo de investigación FaMeTra (Farmacología de la Medicina tradicional y popular), Carrera 30 45-03, Bogotá D.C., Colombia

*Corresponding author. Universidad de Navarra, Facultad de Farmacia y Nutrición, Department of Organic and Pharmaceutical Chemistry, Institute of Tropical Health (ISTUN), Campus Universitario, 31008 Pamplona, Spain. Tel.: +34 948 425600 extension #803329. E-mail address: silvia.galiano@gmail.com (S. Galiano).

[1] Present address: Laboratorio de investigación en Biopolímeros y Metalofármacos, Facultad de Ciencias, Universidad Nacional de Ingeniería, Av. Túpac Amaru 210, Lima 25, Peru

ABSTRACT

Design, synthesis, structure-activity relationship, cytotoxicity studies, *in silico* drug-likeness, genotoxicity screening, and *in vivo* studies of new 1-aryl-3-substituted propanol derivatives led to the identification of nine compounds with promising *in vitro* (**55**, **56**, **61**, **64**, **66**, and **70**-**73**) and *in vivo* (**66** and **72**) antimalarial profiles against *Plasmodium falciparum* and *Plasmodium berghei*. Compounds **55**, **56**, **61**, **64**, **66** and **70**-**73** exhibited potent antiplasmodial activity against chloroquine-resistant strain FCR-3 (IC_{50}s < 0.28 µM), and compounds **55**, **56**, **64**, **70**, **71**, and **72** showed potent biological activity in chloroquine-sensitive and multidrug-resistant strains (IC_{50}s < 0.7 µM for 3D7, D6, FCR-3 and C235). All of these compounds share appropriate drug-likeness profiles and adequate selectivity indexes (77 < SI < 184) as well as lack genotoxicity. *In vivo* efficacy tests in a mouse model showed compounds **66** and **72** to be promising candidates as they exhibited significant parasitemia reductions of 96.4% and 80.4%, respectively. Additional studies such as liver stage and sporogony inhibition, target exploration of heat shock protein 90 of *P. falciparum*, targeted delivery by immunoliposomes, and enantiomer characterization were performed and

strongly reinforce the hypothesis of 1-aryl-3-substituted propanol derivatives as promising antimalarial compounds.

Keywords: Antiplasmodial, Antimalarial, Arylamino alcohol, Multi-stage activity, Hsp90, Enantiomer separation

1. Introduction

Malaria continues to be one of the major tropical diseases affecting the world. According to the latest World Malaria Report produced by the WHO, nearly half of the world's population distributed in 91 countries are at risk of being infected. In 2016 alone, 216 million cases and 445,000 deaths were reported globally, mostly in small African children [1]. The disease is caused by protozoan parasites of the genus *Plasmodium*, with the deadliest being *Plasmodium falciparum* (*P. falciparum*). *Plasmodium*-infected female *Anopheles* mosquitoes bite humans initiating the infection. As a result, the asymptomatic liver stage begins, and newly formed merozoites are released into the bloodstream, where they invade red blood cells, and cause clinical symptoms. Parasite transmission to the mosquito vector occurs when the mosquito ingests circulating gametocytes, and the sexual stage of the parasite`s life cycle is then started [2]. Artemisinin-based combination therapies (ACTs) are currently used as the first-line treatment for this disease [1-3]; however, patients with resistance to artemisinin and its derivatives are routinely identified in Southeast Asia (e.g., along the Cambodia-Thailand border) [3, 4]. Consequently, there is an urgent need for the continued development and innovation of new antimalarial chemical entities targeting the liver stage, sexual forms, and new therapeutic pathways that is being addressed by the academic, industrial and non-profit sectors [5, 6]. Due to the high cost, high rate of

failure and considerable time needed to develop new antimalarial drugs, the study of classic antimalarial drugs or drug repurposing is a promising approach [7, 8].

Present in classic arylamino alcohols (CAA) such as quinine, mefloquine, lumefantrine, and halofantrine, the arylamino alcohol pharmacophore (ß-amino or γ-amino alcohol moiety) is part of the antimalarial arsenal. Mandatory structural features for antiplasmodial activity include the presence of aromatic (AR) and amino alcohol portions linked by a carbon chain of two or three atoms in length [9] (Figure 1).

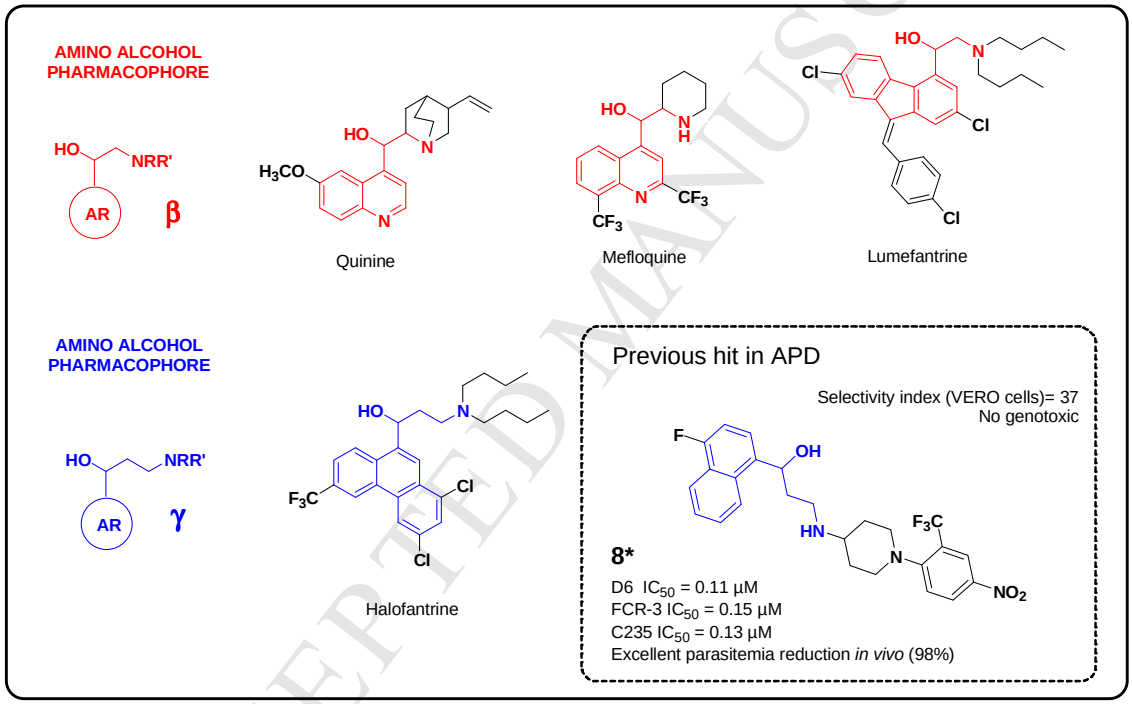

Figure 1. Arylamino alcohol pharmacophores (ß-amino or γ-amino alcohol moiety). Classic arylamino alcohols, APD **8***, and their respective pharmacophores in colors red and blue. Compound **8*** was reported as hit in previous studies [10]

In the last fourteen years, research groups were attracted to the study of aryl amino alcohols due to their high antimalarial activity and ADMET profile. Among them, ß-amino alcohols have been more widely studied in comparison to those with a γ-amino

alcohol moiety. Such studies were listed in our previous publication [10]. In the last months, two new studies explored and identified new amino alcohols as selective inhibitors of the heat shock protein 90 (Hsp90) of *P. falciparum* [11] and the hemozoin formation pathway [12].

Our group has been exploring the structure-activity relationship (SAR) of γ-amino alcohols, more specifically, 1-aryl-3-substituted propanol derivatives (APD), during the last decade [10, 13-15]. Recently, we reported the synthesis, antimalarial evaluation, toxicological studies, and target exploration of thirteen new APD [10]. In the study, the new APD exhibited promising antiplasmodial activity against drug-sensitive (D6 0.11 μM ≤ IC_{50} ≤ 0.49 μM) and multidrug-resistant (FCR-3 0.40 μM ≤ IC_{50} ≤ 14 μM and C235 0.13 μM ≤ IC_{50} ≤ 1.05 μM) strains of *P. falciparum* (blood stage). Adequate *in silico* drug-likeness and the absence of genotoxicity were essential factors to explore the scope of this chemotype series. Among them, compound **8*** (Figure 1) displayed an excellent parasitemia reduction (98 ± 1%) and complete curing of all the treated mice infected with *Plasmodium berghei* (*P. berghei*). However, its selectivity index (SI = 37) remain a priority problem to overcome as well as its unexplored multistage activity. Two important therapeutic targets in the fight against malaria, i.e., the plasmepsin II enzyme of *P. falciparum* and hemozoin inhibition pathway, were explored to establish a mechanism of action, but the targets were discarded; APD may provide an alternative antimalarial mechanism to others arylamino alcohols referenced in the literature. Although our recent results represent a significant advance within APD (the γ-amino alcohol field), more studies are needed to expand, and optimize the chemical series.

In this manuscript, we explored and addressed new assays to reinforce the hypothesis of APD as promising antimalarial compounds. The new exploration and development of APD were performed by: (1) expanding SAR studies using physicochemical, electronic,

bulky and bioisosteric replacements at aromatic regions Ar_1 and Ar_2 (Figure 2), (2) generating additional derivatives with high potency against both chloroquine-sensitive and multidrug resistant strains of *P. falciparum* (blood stage), (3) reducing the cytotoxicity or improving the selectivity index of the most active compounds, (4) improving or maintaining high values of parasitemia reduction in the *P. berghei* mouse model as was exhibited by compound **8*** previously, (5) evaluating multistage activity (liver stage activity and sporogony inhibition), (6) exploring a new biological target in *P. falciparum*, (7) testing new strategies to deliver APD into parasitized red blood cells (pRBCs) as an alternative to oral administration, and (8) exploring antiplasmodial and cytotoxicity profiles on racemic mixtures and individual enantiomers on APD as strategy for future optimizations.

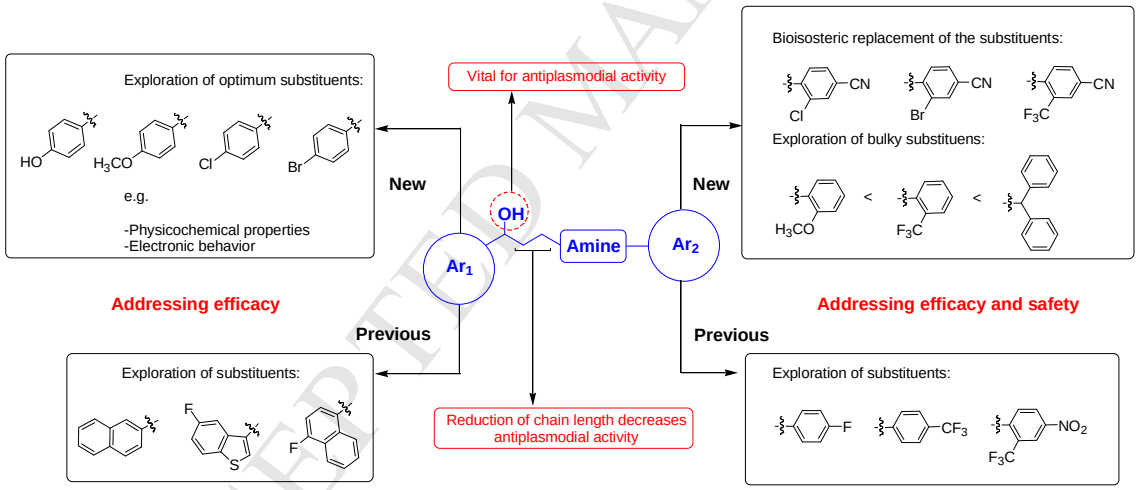

Figure 2. General SAR landscape for APD: Previous and new substitutions in Ar_1 and Ar_2 regions.

2. Results and discussion

2.1. Design criteria for the new APD

The design criteria of the new APD were based on the consensus pharmacophore model proposed by us previously [10]. The model was obtained taking into account the most

active APD reported by our group in which different chemical scaffolds share common structural features, and therefore, a common SAR landscape. The design criteria can be broken down as follows:

2.1.1. Exploration of the Ar_1 region using 4-(4-fluorophenyl)-1,2,3,6-tetrahydropyridine as a common scaffold

A common substituent in the Ar_1 region for APD is an aromatic fragment attached to a fluorine atom. Indeed, our most active compounds previously reported for APD presented 4-fluorophenyl or 4-fluoronaphthyl groups in the Ar_1 region [10, 13]. However, the use of alternative substituents remains unexplored for APD. As was shown in Figure 2, the exploration of an optimum substituent was proposed, considering substituents with electron-donating (OCH_3, OH, OCH_2O) and electron-withdrawing (F, Cl, Br, $COOCH_3$, CN) behaviors, and a lipophilicity contribution (hydrophobic and hydrophilic) to the entire molecule. According to recent *in vitro* studies performed by our group [10], two of the five APD that resulted with FCR-3 IC_{50} values less than 0.7 µM and adequate selectivity index (SI) ($37 \leq SI \leq 244$) presented in their structure the scaffold 4-(4-fluorophenyl)-1,2,3,6-tetrahydropyridine. In fact, the scaffold itself showed moderate antiplasmodial activity (FCR-3 IC_{50} = 8.2 µM). Thus, based on its versatile antiplasmodial activity and easy commercial availability, we decided to explore the Ar_1 region using 4-(4-fluorophenyl)-1,2,3,6-tetrahydropyridine as a common scaffold.

2.1.2. Exploring the versatility of the antiplasmodial scaffold 1-[4-nitro-2-(trifluoromethyl)phenyl]piperidin-4-amine

Another scaffold present in two potent compounds recently studied by us (FCR-3 $IC_{50} \leq$ 0.5 µM, $37 \leq SI \leq 63$) is 1-[4-nitro-2-(trifluoromethyl)phenyl]piperidin-4-amine. These compounds showed marked *in vivo* parasitemia reductions (87-98%), and the scaffold

itself exhibited moderate antiplasmodial activity against the FCR-3 strain (IC_{50} = 4.3 µM) [10]. However, its slow and tedious synthetic route precludes an easy and fast exploration. Taking the above into account and based on the results obtained in section 2.1.1, the exploration of new analogues was performed using the most active and interesting substituents in the Ar_1 region.

2.1.3. Exploring old and new groups in the Ar_2 region

In this section, the SAR information obtained in section 2.1.1 was used to explore the classical groups commonly used at the ortho (CF_3) or para (NO_2 and F) position on the phenyl ring of the Ar_2 region. Additionally, based on the potent antiplasmodial compounds reported by numerous academic groups in which the diphenylmethyl group was used [16-18], the new scaffold was incorporated in the structure of the APD and its versatility was explored.

2.1.4. Decoding the substitutions in the Ar_2 region and their influence on the antiplasmodial activity.

One of the hypotheses used to design new APD was the mandatory presence of a hydrophobic group such as CF_3 at the ortho position on the phenyl ring in the Ar_2 region [10]. However, not only presented the group that physicochemical property but also exhibited an electron-withdrawing behavior. In fact, in our last publications, the predilect substituents used on the phenyl ring in the Ar_2 region were both electron-withdrawing groups (CF_3 and NO_2) [10, 13, 14]. There is only one antecedent where an electron-donating group such as OH was used by us, obtaining a marked decrease in the antiplasmodial activity [14]. This observation led us to ask: 1) is the presence of an electron-withdrawing or hydrophobic group responsible for maintaining the

antiplasmodial activity? and 2) how much could this group contribute to or affect the antimalarial activity compared to aromatic derivatives in region Ar_1? To explore these questions, the OCH_3 group was chosen due to its electron-donating behavior, less lipophilic contribution, structural similarity to the OH group, bulkiness, and synthetic availability. To more effectively compare the analogues, 4-fluorophenyl, 4-fluoronaphthyl and 4-methoxyphenyl groups were used in the Ar_1 region. Additionally, **5***, **6***, and **7*** from our in-house library were tested to establish a clear SAR (contributing long and bulky groups such as phenyl, biphenyl, and 2-naphthyl) [14, 19]. Piperazine and tetrahydropyridine groups were used as amines due to their synthetic accessibility.

*2.1.5. Reducing the cytotoxicity of compound **8*** using bioisostere and non-bioisostere groups*

As previously reported by us, the APD **8*** was used as a reference or starter compound for bioisosteric replacements. Because of its high antiplasmodial activity against drug-sensitive (D6 ≤ 0.19 µM) and multidrug-resistant (FCR-3 ≤ 0.19 µM and C235 ≤ 0.28 µM) strains of *P. falciparum*, excellent parasitemia reduction (98%, *in vivo*) and complete cure of all the treated mice, compound **8*** was considered a promising compound [10]. However, the presence of a nitro group in its structure represents a structural alert always associated with toxicity [20]. Additionally, based on our previous data and pharmacophore model proposed for APD, the presence of a hydrophobic group at the ortho position on the phenyl ring of Ar_2 should ensure the antiplasmodial activity [10, 13]; however, no complementary studies have yet been performed to modulate this structural requirement. Therefore, bioisostere groups on the new APD can be used to 1) maintain high antiplasmodial and antimalarial activity while at the same time improving

the toxicity and thus avoiding future complications related to the presence of the nitro group; 2) modulate the presence of a hydrophobic group at the ortho position on the phenyl ring as mandatory to the antiplasmodial and antimalarial activity. The bioisosteric replacement was performed using Spark™ software [21] containing 536184 commercial fragments from the Zinc database (drug-like) [22]. The results of the Spark™ search showed 1000 possible hits ranked according to their internal scores. The first hit reported was the starter compound **8*** itself, which served as the internal control (Table 1).

Table 1. Selected four hits from Spark experiment. Bioisosteres are ranked according to its internal scores.

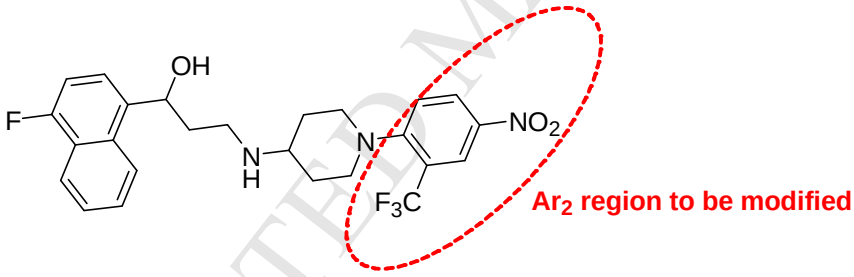

Starter compound

Results	BIF%[a]	Score[b]	Field score[c]	Shape score[d]	ALOGPs 2.1[e]	2D SIM[f]
Hit 1	97	0.992	0.993	0.992	4.39	1
Hit 14	86	0.969	0.956	0.983	4.60	0.752
Hit 128	75	0.945	0.932	0.958	4.91	0.554
Hit 221	72	0.938	0.931	0.946	4.92	0.554

[a]BIF (Bio-Isostere Factor) indicates favorable bioisosteres at geometry, electronic and surface properties; [b]Score, combination of Field and Shape score; [c]Field score, similarity of the result and the starter molecule using only fields excluding shape data; [d]Shape score, similarity of the result and the starter molecule using shapes and excluding all electrostatics data; [e]ALOGPs 2.1 (LogP), logarithm of compound partition coefficient between n-octanol and water; [f]2D SIM, structural similarity of the result and starter molecule, it is used to indicate novelty.

To make more feasible the exploration of the bioisostere groups in the Ar_2 region, filters such as molecular weight (≤ 500 Da), TPSA (≤ 140 $Å^2$), LogP (ALOGPs 2.1 ≤ 5), and

the presence of a nitro group in the final structure were applied to reduce the numbers of hits. Thus, 514 hits were finally obtained and analyzed. Halogen atoms (Br and Cl) and a carbonitrile group at the ortho and para positions, respectively, on the phenyl ring of Ar_2 were found to be the most promising hits to be synthesized based on their ability to mimic the original moiety (BIF%), their similar electrostatic properties (field score), their similar surface properties (shape score) and their novelty (2D SIM or 2D Tanimoto similarity) (Table 1 and Figure 3).

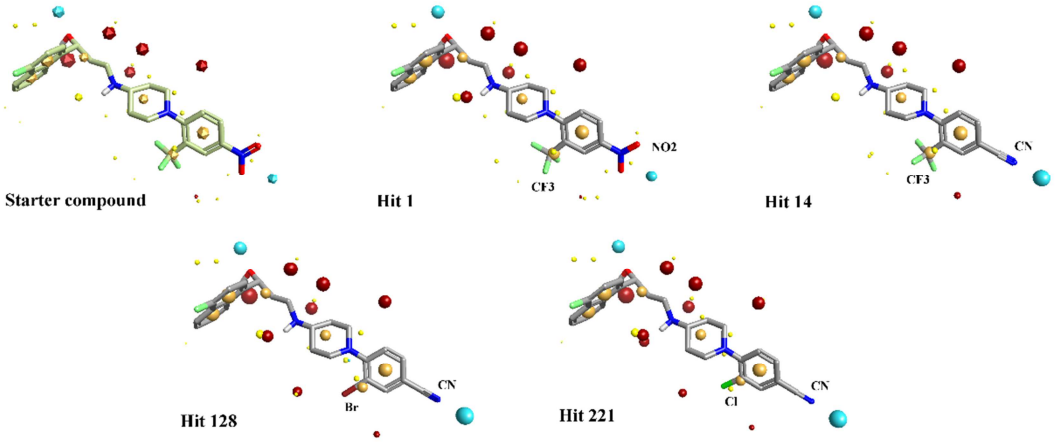

Figure 3. Comparison of the starter compound (**8***) and the 4 selected hits showing the three-dimensional structure and field points (Hit 1, Hit 14, Hit128, and Hit 221). The four field types are represented as follows: red (electrophilic), blue (nucleophilic), orange (hydrophobic), and yellow (van der Waals attractive forces). The size of the field or spheres indicates more energetically favorable interactions can be made.

Therefore, hits 14, 128, and 221 were selected to be synthesized and tested against strains of *P. falciparum*. Of the hit population, the selected hits were ranked among the top 250 of 1000 (without filters) and among the top 70 of 514 (with filters). Finally, a substitution of the NO_2 group by a NH_2 group (non-bioisostere group) was performed to clarify the role of the substituents at the para position on the phenyl ring in the Ar_2 region, a modification in the structure never explored before in APD. In a

complementary way, the synthetic viability was an important criterion used to select the final compounds because the implementation of a new synthetic pathway was not required, consequently obtaining fast results and reducing costs.

2.2. Chemistry

The new APD (**37-73**) were synthesized according to the previous reported procedures [10, 13, 14] outlined in Schemes 1 and 2. The starting arylamines 1-(diphenylmethyl)piperazine, 4-(4-fluorophenyl)-1,2,3,6-tetrahydropyridine, 1-(4-fluorophenyl)piperazine, 1-(2-nitrophenyl)piperazine, 1-(4-nitrophenyl)piperazine, 1-(2-trifluoromethylphenyl)piperazine, 1-(2-methoxyphenyl)piperazine, and 4-(2-methoxyphenyl)-1,2,3,6-tetrahydropyridine (**IVa-g**) were commercially available. Non-commercially available arylamines (**IIIa-d**) were synthesized using 4-(*N*-Boc-amino)piperidine and the corresponding fluorinated derivatives (**Ia-d**) such as 2-fluoro-5-nitrobenzotrifluoride, 3-bromo-4-fluorobenzonitrile, 3-chloro-4-fluorobenzonitrile, and 4-fluoro-3-(trifluoromethyl)benzonitrile by a nucleophilic aromatic substitution reaction (S_NAr) via Meisenheimer complex formation and the later removal of the Boc-group with hydrochloric acid (HCl) and acetic acid (AcOH) (Scheme 1.ii). All methyl ketone compounds (**V**) were commercially available. The ketone intermediates (β-amino ketones) (**1-36**) were prepared using the Mannich reaction (Scheme 1.iii) that involved the condensation of the corresponding methyl ketone (**V**) with different aryl amines (**IIIa-d** and **IVa-g**). The final hydroxyl derivatives (γ-amino alcohols) (**37-72**) were synthesized by the reduction of the corresponding carbonyl group with sodium borohydride ($NaBH_4$) in methanol (MeOH) (Scheme 1.iv). The final hydroxyl compound **73** was obtained by the reduction of the aromatic nitro group to an amine

with hydrazine monohydrate and Raney nickel as catalyst in the presence of MeOH using as an intermediate the previously published compound **VI** (Scheme 2.i) [10].

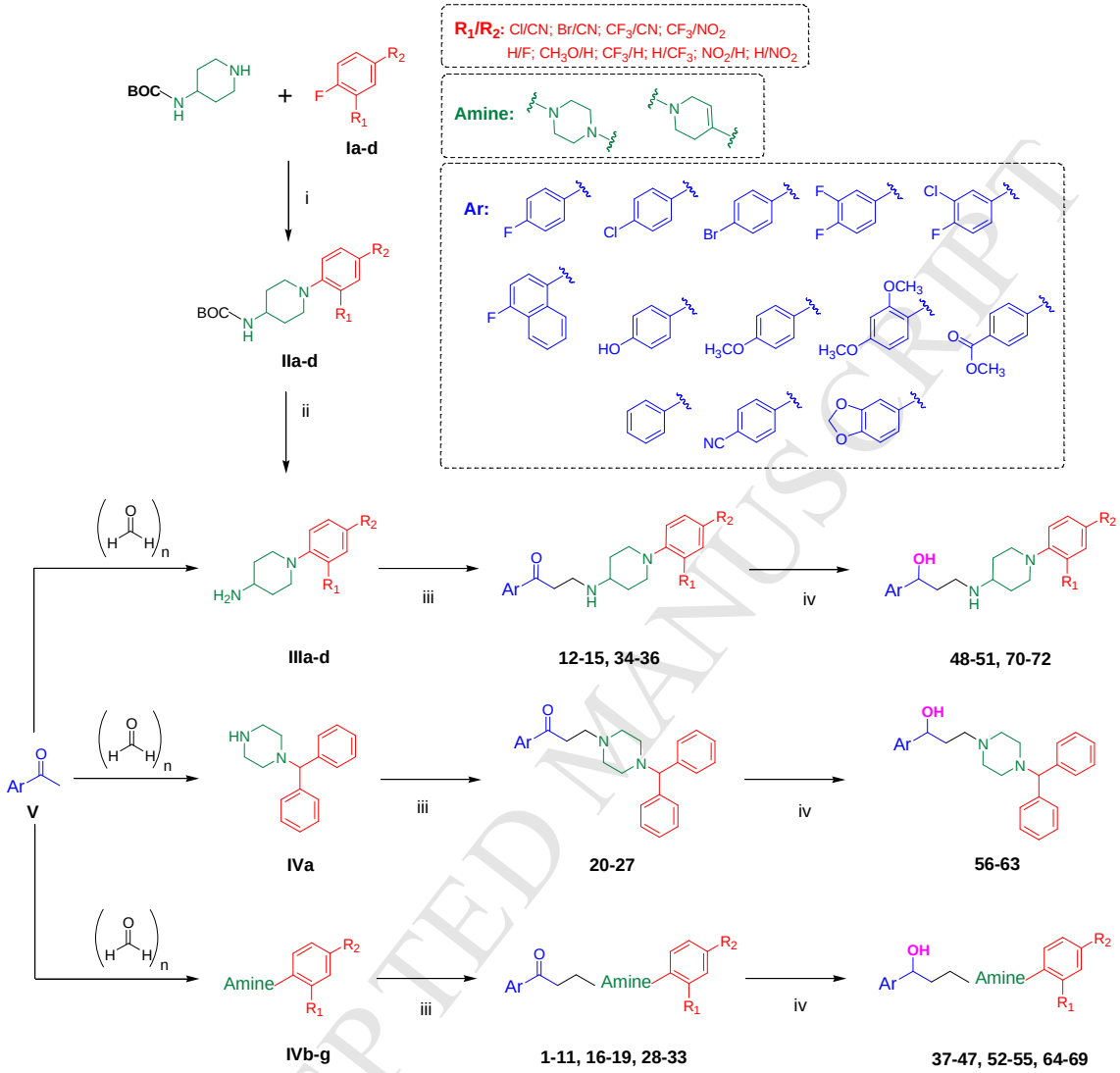

Reagents and conditions: (i) CH_3CN, K_2CO_3, 12 h, reflux; (ii) AcOH / HCl (1:1), rt., 2 h, NaOH 2M; (iii) 1,4-dioxane, microwaves, 5 min, 100-110 ^oC, 20 PSI, 150 W; (iv) MeOH, $NaBH_4$, 0 ^oC, 2 h

Scheme 1. Synthesis of arylamino alcohols **37-72**

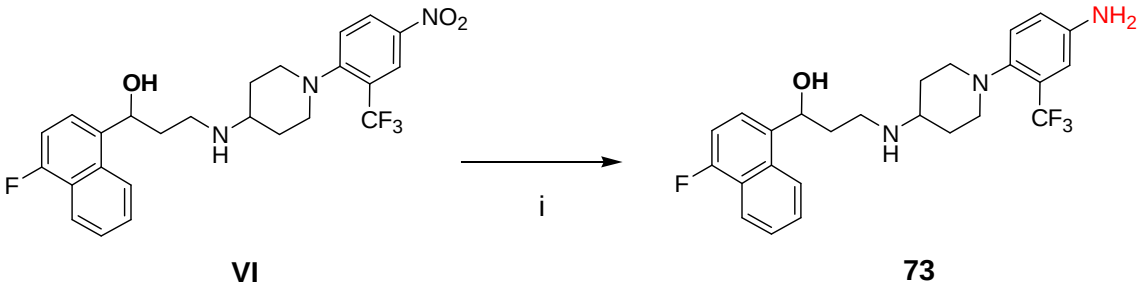

VI **73**

Reagents and conditions: (i) MeOH, 0 ^{o}C, Raney nickel, hydrazine monohydrate, 3 h

Scheme 2. Synthesis of arylamino alcohol **73**

2.3. In vitro antiplasmodial activity (3D7 and FCR-3 strain) and cytotoxicity studies.

The activities of thirty-seven new synthesized hydroxyl analogues (**37-73**) were determined against the 3D7 chloroquine-sensitive strain and FCR-3 multidrug-resistant strain of *P. falciparum* (Tables 2-7). Chloroquine was used as a reference drug in all experiments for comparison (3D7 IC_{50} = 0.02, FCR-3 IC_{50} = 0.12 µM). Their cytotoxicity was determined against HepG-2 cells.

2.3.1. Exploration of Ar_1 region using 4-(4-fluorophenyl)-1,2,3,6-tetrahydropyridine as a common scaffold

The antiplasmodial activities of eleven newly synthesized hydroxyl analogues (**37-47**) are shown in Table 2. Although none of the compounds showed submicromolar activity against the strains (IC_{50} < 1 µM), compounds **40-43** exhibited similar antiplasmodial activities against the 3D7 (2.27 µM ≤ IC_{50} ≤ 5.42 µM) and FCR-3 strains (2.01 µM ≤ IC_{50} ≤ 7.06 µM). On the contrary, compounds **37-39** and **45-47** showed significant differences in potency between strains (e.g., **39** 3D7 IC_{50} = 17.38 µM vs. FCR-3 IC_{50} = 1.70). Overall, compounds **40, 41, 42**, and **43** were the most active compounds against the 3D7 strain (2.27 µM ≤ IC_{50} ≤ 5.42 µM), while for the FCR-3 strain, compounds **37-39**, **41-43**, and **47** were the most active (1.13 µM ≤ IC_{50} ≤ 2.88 µM). In both cases, moderate antiplasmodial activity was exhibited (1 µM ≤ IC_{50} ≤ 10 µM). An analysis of the results obtained shows that the different substitutions on the phenyl ring of the Ar_1

region did not contribute to the increase of the antiplasmodial activity in comparison with the previous analogues synthesized, where IC_{50} values of 0.66 and 0.40 µM were reported for 4-fluorophenyl and 4-fluoronaphthyl, respectively [10]. Additionally, it must be highlighted that the presence of halogen atoms, such as Br, Cl, and F, increases the antiplasmodial activity (F > Cl > Br) and contributes to maintaining the potency in both strains.

Table 2. *In vitro* antimalarial activity against chloroquine sensitive strain (3D7) and multidrug-resistant strain (FCR-3) of *P. falciparum*, and HepG-2 cytotoxicity of compounds **37-47**

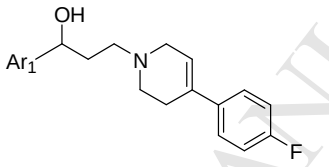

Compound	Ar_1	IC_{50} (µM)[a] *P. falciparum*		CC_{50}(µM)[b]	SI[c]
		3D7	FCR-3	HepG-2[d]	
37	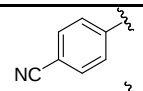	8.48 ± 1.40	1.33 ± 0.20	82.43 ± 4.00	62
38	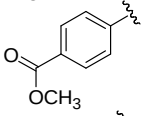	10.46 ± 3.40	1.13 ± 0.50	509.30 ± 19.80	451
39	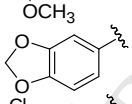	17.38 ± 4.70	1.70 ± 0.20	164.88 ± 23.10	97
40	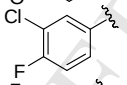	2.27 ± 0.20	7.06 ± 1.70	54.08 ± 4.60	8
41	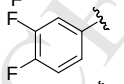	2.79 ± 0.90	2.01± 0.60	96.97 ± 16.20	48
42	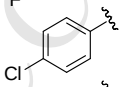	3.57 ± 0.50	2.29 ± 0.20	109.81± 15.40	48
43	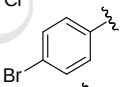	5.42 ± 1.30	2.68 ± 0.50	108.58 ± 2.40	41
44		10.64 ± 1.40	9.04 ± 0.80	121.15 ± 9.10	13
45	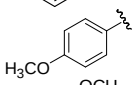	18.25 ± 5.80	11.54 ± 0.10	151.94 ± 4.30	13
46	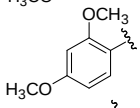	24.09 ± 1.40	9.48 ± 1.00	91.36 ± 3.00	10
47	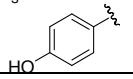	22.17 ± 2.10	2.88 ± 0.10	253.23 ± 10.90	88
CQ[e]	-	0.02	0.12	137.49	1146

[a]IC_{50}: Concentration that produces 50% of the inhibitory effect.

[b]CC_{50}: Concentration that produces 50% of cytotoxicity.
[c]SI: Selectivity index = CC_{50} HepG-2 cells/ FCR-3 IC_{50} *P. falciparum*.
[d]HepG-2: Human hepatocellular carcinoma cells.
[e]CQ: chloroquine.

2.3.2. Exploring the versatility of the antiplasmodial scaffold 1-[4-nitro-2-(trifluoromethyl)phenyl]piperidin-4-amine

Based on the SAR information obtained in the exploration of the Ar_1 region (section 2.3.1), the introduction of F, Cl, and CN substituents was chosen to explore new analogues. The antiplasmodial activities of four newly synthesized hydroxyl analogues (**48-51**) are shown in Table 3. Compounds **48** and **49** containing halogen atoms (Cl and F) were found to be the most active compounds in this series showing marked antiplasmodial activity in both strains, and almost equaling the antiplasmodial activity previously shown by the synthesized compound **1*** (FCR-3 IC_{50} = 0.48 µM) [10]. No substitution (**50**) or introduction of a carbonitrile group on the phenyl group (**51**) led to a drop in potency.

Table 3. *In vitro* antimalarial activity against chloroquine sensitive strain (3D7), and multidrug-resistant strain (FCR-3) of *P. falciparum*, and HepG-2 cytotoxicity of compounds **48-51**

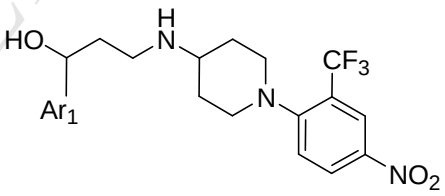

Compound	Ar_1	IC_{50} (µM)[a] *P. falciparum*		CC_{50} (µM)[b]	SI[c]
		3D7	FCR-3	HepG-2[d]	
48	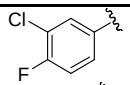	0.71 ± 0.20	0.51 ± 0.02	4.61 ± 0.04	9
49	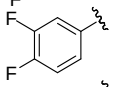	0.67 ± 0.10	0.53 ± 0.08	13.33 ± 1.70	25
50	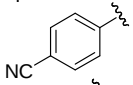	4.22 ± 2.90	2.02 ± 0.20	23.0 ± 2.80	11
51		4.42 ± 0.20	1.80 ± 0.50	27.63 ± 0.20	15

1*	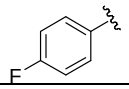	ND[f]	0.48 ± 0.04	10.40 ± 1.60	22
CQ[e]	-	0.02	0.12	137.49	1146

[a]IC_{50}: Concentration that produces 50% of the inhibitory effect.
[b]CC_{50}: Concentration that produces 50% of cytotoxicity.
[c]SI: Selectivity index = CC_{50} HepG-2 cells/ FCR-3 IC_{50} *P. falciparum*.
[d]HepG-2: Human hepatocellular carcinoma cells
[e]CQ: chloroquine.
[f]ND: Not determined.
*Previously synthesized by our group [10]

2.3.3. Exploring old and new groups in the Ar_2 region

To expand the landscape in the Ar_2 region, different substitutions on the phenyl ring attached to a piperazine were carried out. In this series, 4-fluoronaphthyl was introduced in the Ar_1 region according to the SAR shown in section 2.3.1. The activities of five newly synthesized hydroxyl analogues (**52-56**) are shown in Table 4. Compounds **55** and **56** were the most potent APD, with comparable submicromolar values for both strains. In contrast, the rest of the compounds within this series displayed significant differences between the two strains, with compounds **52** and **53** achieving submicromolar values for the 3D7 strain. In this new exploration, the complete SAR data are revealed for electron-withdrawing substituents at the ortho and para positions on the phenyl ring such as CF_3, NO_2, and F. These groups had been previously tested by our group in different positions and combinations (e.g., the reference compounds **2*-4***) [10, 13], but the exact role of each one had not been clarified (e.g., electrostatic, steric, lipophilic). The removal of the CF_3 group at the ortho position maintaining the NO_2 group at the para position led to a decrease in antiplasmodial activity (**54** FCR-3 IC_{50} = 1.71 µM vs. **4*** FCR-3 IC_{50} = 0.5 µM). In contrast, an improvement of the antiplasmodial efficacy was achieved with the corresponding *o*-CF_3 analogue in which the NO_2 group had been removed (**55** FCR-3 IC_{50} = 0.15 µM vs. **4*** FCR-3 IC_{50} = 0.5 µM). This last improvement is also observed in the case of the NO_2 group at the ortho position and the CF_3 group removed from the para position (**53** FCR-3 IC_{50} = 2.62 µM

vs. **3*** FCR-3 IC_{50} = 5.0 µM). Additionally, when a CF_3 group is substituted at the para position for a NO_2 or F group, the activity decreases. Therefore, our data reinforces our previous 3D pharmacophore model, in which the presence of a hydrophobic group is necessary to obtain potent antimalarial compounds against chloroquine-resistant strain FCR-3. It must be noticed that bulky groups (e.g., NO_2) at the ortho position retained antiplasmodial activity in chloroquine-sensible strain 3D7 even if they are not hydrophobic. However, the electronic role of the substituents at the ortho and para positions remains unsolved. On the other hand, a novel scaffold 1-(diphenylmethyl)piperazine was incorporated in the structure of APD, and its versatility was explored in the following section.

Table 4. *In vitro* antimalarial activity against chloroquine sensitive strain (3D7) and multidrug-resistant strain (FCR-3) of *P. falciparum*, and HepG-2 cytotoxicity of compounds **52-56**

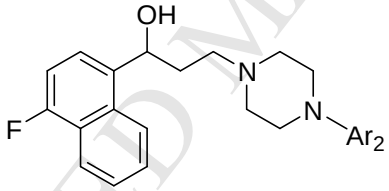

Compound	Ar_2	IC_{50} (µM)[a] *P. falciparum*		CC_{50} (µM)[b]	SI[c]
		3D7	FCR-3	HepG-2[d]	
52	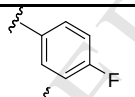	0.43 ± 0.10	4.05 ± 1.40	29.38 ± 4.30	7
53	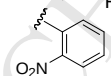	0.92 ± 0.30	2.62 ± 0.30	19.86 ± 0.40	8
54	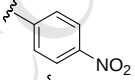	4.74 ± 0.40	1.71 ± 0.60	12.47 ± 1.10	7
55	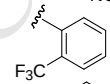	0.16 ± 0.06	0.15 ± 0.03	27.52 ± 0.60	183
56	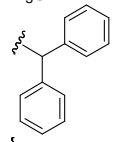	0.62 ± 0.02	0.33 ± 0.04	19.90 ± 2.70	60
2*	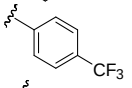	ND[f]	0.93 ± 0.70	ND	-
3*	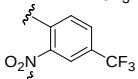	ND	5 ± 0.08	ND	-
4*	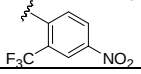	ND	0.5 ± 0.02	ND	-
CQ[e]	-	0.02	0.12	137.49	1146

[a]IC_{50}: Concentration that produces 50% of the inhibitory effect.
[b]CC_{50}: Concentration that produces 50% of cytotoxicity.
[c]SI: Selectivity index = CC_{50} HepG-2 cells/ FCR-3 IC_{50} *P. falciparum*.
[d]HepG-2: Human hepatocellular carcinoma cells
[e]CQ: chloroquine.
[f]ND: Not determined.
[*]Previously synthesized by our group [10, 13]

2.3.3.1. Exploration of the 1-(diphenylmethyl)piperazine scaffold

Encouraged by the potent activity of compound **56** bearing a 1-(diphenylmethyl)piperazine scaffold against both strains (3D7 IC_{50} = 0.62 µM and FCR-3 IC_{50} = 0.33 µM), we decided to expand this chemical series using the most active variations used in the Ar_1 region. The antiplasmodial activities of seven newly synthesized hydroxyl analogues (**57-63**) are shown in Table 5. Compounds containing fluorine atoms were the most active (**57** and **61)**. Compounds **58-60**, **62**, and **63** showed moderate to low antiplasmodial activity (1 µM ≤ IC_{50}s ≤ 52 µM). From a structural point of view, the new scaffold meets the requirement of having a hydrophobic portion in the Ar_2 region, which is important for the antiplasmodial activity [10]. The use of the substituents 4-fluoronaphthyl and 3,4-fluorophenyl in the Ar_1 region showed almost the same IC_{50} values for both strains (**56** vs. **61**; IC_{50}s ≤ 0.62 µM). Interestingly, the same substituents reported a similar modulation of the antiplasmodial activity using the 1-[4-nitro-2-(trifluoromethyl)phenyl]piperidin-4-amine scaffold (**49** vs. **8***; IC_{50}s ≤ 0.67 µM). In contrast, the substituents 4-fluoronaphthyl and 3,4-fluorophenyl with the 4-(4-fluorophenyl)-1,2,3,6-tetrahydropyridine as a common scaffold did not show this pattern (a scaffold without a hydrophobic group at ortho position in the Ar_2 region). Thus, 3,4-fluorophenyl can be considered a good alternative to classical groups such as 4-fluoronaphthyl and 4-fluorophenyl when chemical scaffolds containing a hydrophobic group in the Ar_2 region are used.

Table 5. *In vitro* antimalarial activity against chloroquine sensitive strain (3D7) and multidrug-resistant strain (FCR-3) of *P. falciparum*, and HepG-2 cytotoxicity of compounds **57-63**

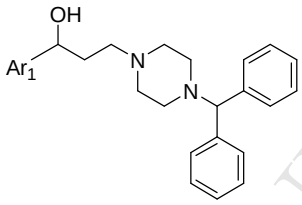

Compound	Ar_1	IC_{50} (µM)[a] *P. falciparum*		CC_{50} (µM)[b]	SI[c]
		3D7	FCR-3	HepG-2[d]	
57	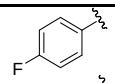	1.08 ± 0.04	0.62 ± 0.20	252 ± 20.60	406
58	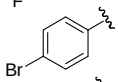	52.22 ± 6.80	3.09 ± 0.20	351.40 ± 27.70	114
59	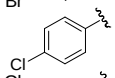	24.85 ± 4.90	3.93 ± 1.10	462.43 ± 2.20	118
60	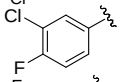	5.11 ± 0.30	1.39 ± 0.40	269.16 ± 2.10	194
61	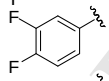	0.38 ± 0.07	0.37 ± 0.02	54.27 ± 6.90	147
62	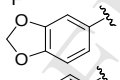	1.66 ± 0.04	1.44 ± 0.20	36.10 ± 4.80	25
63	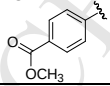	1.69 ± 0.06	1.46 ± 0.20	83.96 ± 5.30	58
CQ[e]	-	0.02	0.12	137.49	1146

[a]IC_{50}: Concentration that produces 50% of the inhibitory effect.
[b]CC_{50}: Concentration that produces 50% of cytotoxicity.
[c]SI: Selectivity index = CC_{50} HepG-2 cells/ FCR-3 IC_{50} *P. falciparum*.
[d]HepG-2: Human hepatocellular carcinoma cells
[e]CQ: chloroquine.

2.3.4. Decoding the substitutions in the Ar_2 region and their influence on the antiplasmodial activity

The activities of six newly synthesized hydroxyl analogues (**64-69**) are shown in Table 6. Substitutions in the Ar_2 region on the phenyl ring at the ortho position by CF_3

and OCH_3 groups while maintaining the 4-fluorophenyl group in the Ar_1 region and piperazine as the amine showed potent to moderate activity against both strains (**66** and **68**, 0.19 µM ≤ IC_{50}s ≤ 7.31 µM). Meanwhile, when a 4-fluoronaphthyl group replaces 4-fluorophenyl on the left hand side of these derivatives, both compounds exhibited potent activity (**55** and **64**; 3D7 and FCR-3 IC_{50}s ≤ 0.22 µM). Therefore, the SAR analysis revealed that the essential structural requirement for antiplasmodial activity at the ortho position was the presence of groups with a hydrophobic surface and a bulky nature (e.g., CF_3, OCH_3), regardless of the electronic nature of the substituents (electron-withdrawing or electron-donating). For example, compound **53** with a bulky NO_2 group but no hydrophobic surface led to a decrease in the antiplasmodial activity in comparison with compounds **55** and **64** (Figure 4).

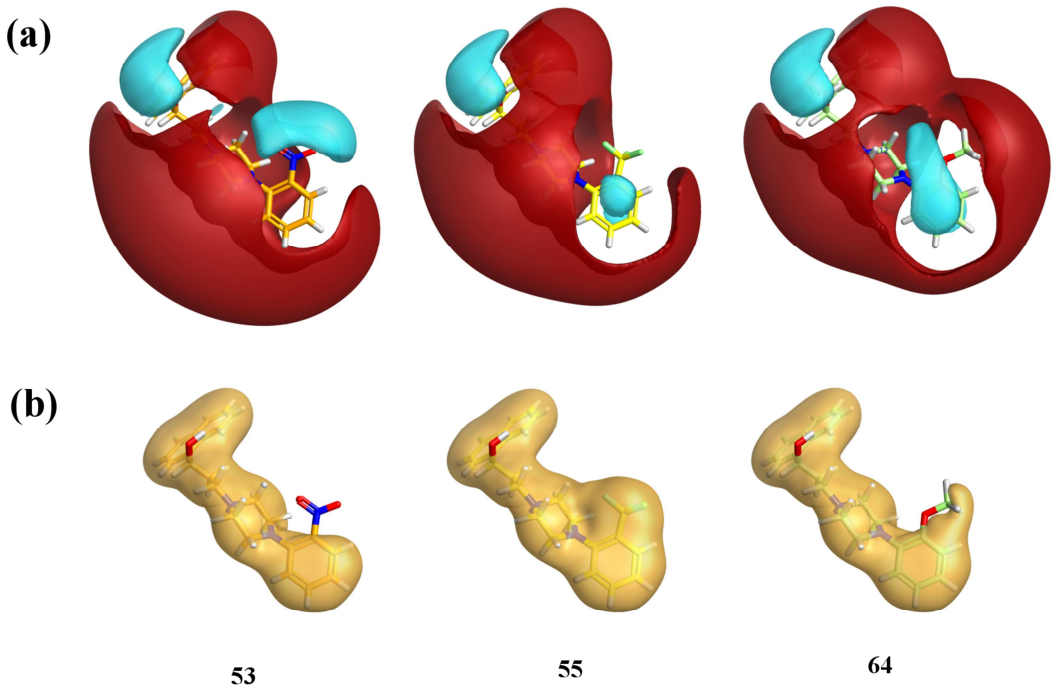

Figure 4. Electrostatic and hydrophobic surfaces for compounds **53**, **55**, and **64**. (a) Negative (cyan) and positive (red) electrostatic surface; (b) hydrophobic surface (orange). The change of substituents at ortho position on the phenyl ring in the Ar_2

region introduce negative charges but also withdraws or donates electrons from the ring modifying the positive charge of aromatic hydrogens

As a second approach, the comparison of compounds **66**, **69**, **5***, **6***, and **7*** clearly shows that the presence of the OCH_3 group itself in the Ar_2 region did not guarantee potent antimalarial activity. By contrast, the absence of a hydrophobic surface or bulky substituent at the ortho position in cases where 4-fluorophenyl and 4-fluoronaphthyl were present in the Ar_1 region was partially tolerated, reaching moderate to potent antimalarial activity against at least one strain of *P. falciparum* (e.g., compounds **52**, **53**, **2***). Finally, the comparison of piperazine and tetrahydropyridine groups as the central amine (**64** vs. **65** and **66** vs. **67**) indicates that piperazine analogues are more active than tetrahydropyridine analogues against FCR-3 strain.

Table 6. *In vitro* antimalarial activity against chloroquine sensitive strain (3D7) and multidrug-resistant strain (FCR-3) of *P. falciparum*, and HepG-2 cytotoxicity of compounds **64-69**

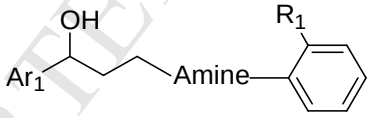

Compound	Ar_1	Amine	R_1	IC_{50} (μM)[a] *P. falciparum*		CC_{50} (μM)[b]	SI[c]
				3D7	FCR-3	HepG-2[d]	
64	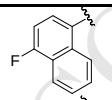	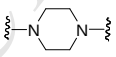	OCH_3	0.07 ± 1.60	0.22 ± 0.02	30.37 ± 5.40	138
65	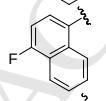	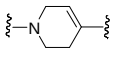	OCH_3	0.10 ± 1.90	1.30 ± 0.20	17.69 ± 3.10	14
66	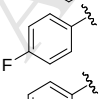	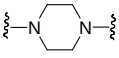	OCH_3	7.31 ± 0.02	0.19 ± 0.10	19.54 ± 0.02	103
67	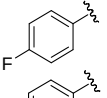	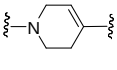	OCH_3	2.82 ± 9.10	1.32 ± 0.02	67.03 ± 9.10	51
68	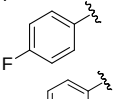	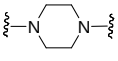	CF_3	1.01 ± 0.10	1.69 ± 0.40	1.35 ± 0.18	1
69	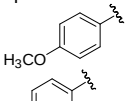	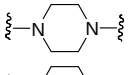	OCH_3	10.53 ± 1.20	7.98 ± 1.20	370.83 ± 33.30	46
5*		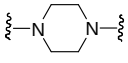	OCH_3	13.90 ± 0.90	15.66 ± 1.20	> 612	> 39

6*	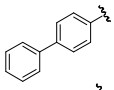	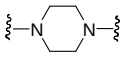	OCH_3	7.25 ± 2.80	2.78 ± 0.02	24.44 ± 4.30	9
7*	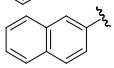	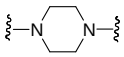	OCH_3	4.08 ± 1.60	2.63 ± 0.10	95.01 ± 4.20	36
CQ[e]	-	-	-	0.02	0.12	137.49	1146

[a]IC_{50}: Concentration that produces 50% of the inhibitory effect.
[b]CC_{50}: Concentration that produces 50% of cytotoxicity.
[c]SI: Selectivity index = CC_{50} HepG-2 cells/ FCR-3 IC_{50} *P. falciparum*.
[d]HepG-2: Human hepatocellular carcinoma cells.
[e]CQ: chloroquine.
[*]Previously synthesized by our group [14, 19]

2.3.5. Reducing the cytotoxicity of compound 8 using bioisostere and non-bioisostere groups*

Based on the detailed criteria used to design new analogues of compound **8*** (see section 2.1.5.), the activities of four newly synthesized hydroxyl analogues (**70**-**73**) are shown in Table 7. Compounds **70**-**73** exhibited IC_{50} values below 0.1 µM against the FCR-3 strain and IC_{50} values below 0.22 µM against the 3D7 strain. As was expected for compounds **70**-**72**, the use of the bioisosteric replacements generated analogues with similar antimalarial potency against *P. falciparum*, while the cytotoxicity of HepG-2 was attenuated (for a more in-depth discussion of the cytotoxicity, see section 2.3.6.). Interestingly, hydrophobic groups of different sizes (Cl < Br < CF_3) at the ortho position were well tolerated. Although compound **73** had an electron-donating group (NH_2) at the para position on the phenyl ring in the Ar_2 region, the antimalarial potency of the molecule was maintained against both strains ($IC_{50} \leq 0.14$ µM). This observation modifies our previous hypothesis in which only electron-withdrawing groups at the para position contributed to the activity [10]. In fact, the para position can be used to introduce groups that help to improve the water solubility in future optimization campaigns.

Table 7. *In vitro* antimalarial activity against chloroquine sensitive strain (3D7) and multidrug-resistant strain (FCR-3) of *P. falciparum*, and HepG-2 cytotoxicity of compounds **70**-**73**

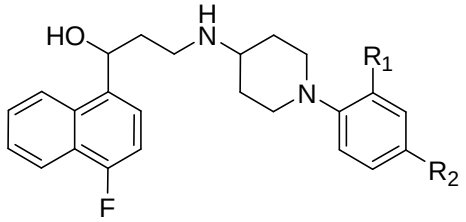

Compound	R_1	R_2	IC_{50} (μM)[a] *P. falciparum*		CC_{50} (μM)[b]	SI[c]
			3D7	FCR-3	HepG-2[d]	
70	Br	CN	0.22 ± 0.10	0.07 ± 0.00	9.87 ± 2.70	141
71	Cl	CN	0.15 ± 0.01	0.09 ± 0.06	7.95 ± 1.20	88
72	CF_3	CN	0.13 ± 0.01	0.08 ± 0.03	6.22 ± 0.60	78
73	CF_3	NH_2	0.14 ± 0.06	0.08 ± 0.00	10.95 ± 0.60	137
8*	CF_3	NO_2	ND[f]	0.15 ± 0.01	5.70 ± 1.80	38
CQ[e]	-	-	0.02	0.12	137.49	1146

[a]IC_{50}: Concentration that produces 50% of the inhibitory effect.
[b]CC_{50}: Concentration that produces 50% of cytotoxicity.
[c]SI: Selectivity index = CC_{50} HepG-2 cells/ FCR-3 IC_{50} *P. falciparum*.
[d]HepG-2: Human hepatocellular carcinoma cells
[e]CQ: Chloroquine.
[f]ND: Not determined.
[*]Previously synthesized by our group [10]

2.3.6. General cytotoxicity

The cytotoxicities of the thirty-seven newly synthesized hydroxyl analogues (**38**-**73**) were determined against HepG2-A16 cells using the MTT assay [23] (Tables 2-7). An exploration of the Ar_1 region showed that compounds with substituents on the phenyl ring containing halogen atoms such as F, Cl, or Br (**41**-**43**) exhibited a moderate selectivity index ($41 \leq SI \leq 48$), except for compound **40** (low SI = 8). Meanwhile, substituents such as CN, $COOCH_3$, $-OCH_2O-$, and OH resulted in a moderate to high selectivity index ($62 \leq SI \leq 451$). Unsubstituted phenyl ring and OCH_3 groups resulted in a significant drop in SI (**44**, **45**, and **46**). The use of the different Ar_1 substituents with the 1-[4-nitro-2-(trifluoromethyl)phenyl]piperidin-4-amine scaffold did not improve on the SI of the previous analogue compound **1*** (SI = 22). Compound **49** was the only analogue with a similar SI (**49** SI = 25). Therefore, the 3,4-difluoro substitution on the phenyl ring of the Ar_1 region can be considered an alternative variation because of the moderate SI presented in APD. On the other hand, the cytotoxicity exploration of the Ar_2 region showed that compounds **55** and **56,** bearing trifluoromethyl and

diphenylmethyl groups, respectively, exhibited high to moderate SI ($183 \geq SI \geq 60$). In fact, the high selectivity of the diphenylmethyl scaffold is reinforced by compounds **57-63,** which exhibited moderate to high SI ($25 \geq SI \geq 406$), even though variations in the Ar_1 region were responsible for the low selectivity in other series (**40** vs. **48** vs. **60**). High selectivity was also observed for compound **64** (OCH_3; $SI \geq 100$), which is a structural analogue of compound **55** (CF_3). A comparison between the piperazine and tetrahydropyridine groups showed that analogues with piperazine as the central amine are less cytotoxic than tetrahydropyridine (**64** vs. **65** and **66** vs. **67**). The use of bioisostere and non-bioisostere groups allowed us to obtain new analogues of compound **8*** with a marked decrease in cytotoxicity (**70-73**). Taking as a starting point the SI of compound **8*** (SI = 38), high values of selectivity were reached for analogues **70-73** ($78 \leq SI \leq 141$). This increase in the SI values can be explained by the absence of the nitro group and its well-documented mutagenic and carcinogenic potential [20]. The most remarkable result to emerge from the bioisosteric replacement is the feasibility of obtaining a high selectivity using the aminopiperidine scaffold ($SI \geq 78$). In fact, in our previous studies, because of its high antiplasmodial activity, the aminopiperidine scaffold was considered an attractive fragment, but its selectivity was always of concern [10, 14].

2.4. In vitro antiplasmodial activity (D6 and C235 strains)

As part of our antimalarial drug discovery pipeline, new APD must exhibit remarkable potency against both chloroquine-sensitive and multidrug-resistant strains of *P. falciparum*. More specifically, the objective is to explore and establish a broad spectrum of antiplasmodial efficacy for new APD against mefloquine-resistant strains. Mefloquine, a classical arylamino alcohol, is a molecule widely used by the WHO in

chemoprotection campaigns [1, 2]. Therefore, nine compounds with marked antiplasmodial activities (FCR-3 $IC_{50} \leq 1.32$ μM) were independently evaluated and validated in two laboratories using two different strains of *P. falciparum*. The newly synthesized APD were tested against the D6 chloroquine-sensitive (but naturally less susceptible to mefloquine) and C235 multidrug-resistant strains (resistant to mefloquine, chloroquine, and pyrimethamine) (Table 8). All the selected compounds except **66** and **67** exhibited potent antimalarial activity against both strains (D6 $IC_{50} \leq$ 0.28 μM, C235 $IC_{50} \leq 0.41$ μM). Compounds **55** and **72** were found to be the most active compounds, with IC_{50} values in the range of 0.08-0.14 μM for the D6 and C235 strains. Based on our results and previous IC_{50} data against the D6 and C235 strains [10], it is clear that, in general, the substituent 4-fluoronaphthyl was present in the Ar_1 region in the most active compounds. Such a characteristic can be observed more clearly if the analogues using 4-fluoronaphthyl and 4-fluorophenyl are compared (**64** vs. **66** and **65** vs. **67**). Our results reinforce the idea that APD have remarkable potency against chloroquine-sensitive (3D7 and D6) and multidrug-resistant (FCR-3 and C235) strains of *P. falciparum*.

Table 8. *In vitro* antimalarial activity against chloroquine sensitive strain (D6) and multidrug-resistant strain (C235) of *P. falciparum*

Compound	Structure	IC_{50} (μM)[a] *P. falciparum*	
		D6	C235
55	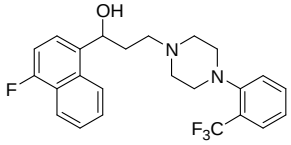	0.10 ± 0.01	0.14 ± 0.01
56	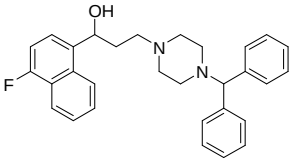	0.10 ± 0.02	0.17 ± 0.01

64	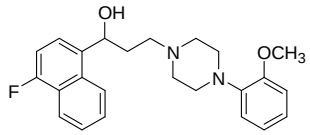	0.28 ± 0.03	0.41 ± 0.00
65	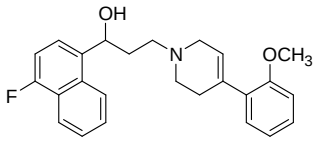	0.15 ± 0.01	0.23 ± 0.00
66	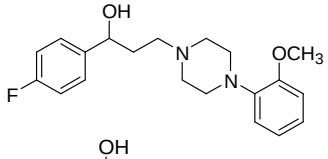	6.32 ± 0.33	7.26 ± 0.17
67	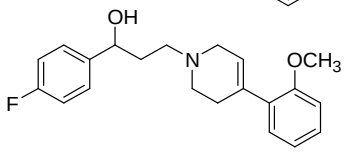	3.73 ± 0.43	3.69 ± 0.17
70	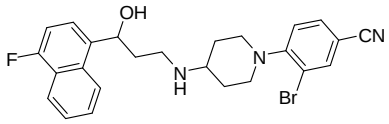	0.12 ± 0.00	0.15 ± 0.01
71	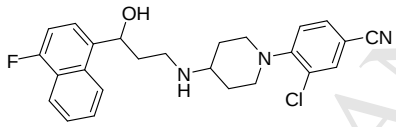	0.12 ± 0.00	0.17 ± 0.02
72	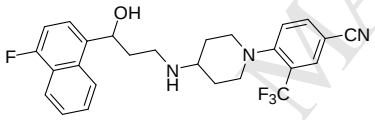	0.08 ± 0.00	0.12 ± 0.02
CQ		0.01 ± 0.00	0.05 ± 0.00

[a]IC_{50}: Concentration that produces 50% of the inhibitory effect.

2.5. In silico physicochemical properties and druglikeness evaluation

An *in silico* study was performed for the prediction of the druglikeness profile of synthesized APD (Table 9). Used as a good descriptor of the drug absorbance in the intestines, blood-brain barrier crossing, and Caco-2 monolayer penetration the topological polar surface area (TPSA) was calculated [24], and the theoretical percentage of human intestinal absorption (%ABS) was obtained according to the equation %ABS = 109 – 0.345 x TPSA [25]. Additionally, the number of rotatable bonds (n-ROTB) were calculated, and the druglikeness profile according to Lipinski's rule of five [26] and Veber's rule [27] was evaluated for APD. From these parameters, all compounds exhibited a %ABS ranging between 80 to 100%, except for compound

50 (73%). Only compounds **56** and **60** violated one Lipinski parameter, and no compounds violated Veber's rule. Therefore, the oral bioavailability of the APD synthesized can be considered promising for further development as agents for antimalarial therapy.

Table 9. *In silico* physicochemical properties of tested APD (ADME profile)

ID	TPSA (Å^2)[a]	%ABS[b]	n-ROTB[c]	MW[d]	ALOGPs2.1[e]	n-OHNH donors[f]	n-ON acceptors[g]	LV[h]
Rule	**≤ 140**		**≤ 10**	**< 500**	**< 5**	**< 5**	**< 10**	**≤ 1**
37	47.3	93	5	336.40	3.51	1	4	0
38	49.8	92	7	369.43	3.85	1	5	0
39	41.9	95	5	355.40	3.00	1	5	0
40	23.5	100	5	363.83	4.56	1	4	0
41	23.5	100	5	347.37	3.93	1	5	0
42	23.5	100	5	345.84	4.53	1	3	0
43	23.5	100	5	390.29	4.44	1	3	0
44	23.5	100	5	311.39	4.06	1	3	0
45	32.7	98	6	341.42	3.88	1	4	0
46	41.9	95	7	371.45	3.79	1	5	0
47	43.7	94	5	327.39	3.67	2	4	0
48	81.3	81	8	475.86	3.98	2	8	0
49	81.3	81	8	459.41	3.57	2	9	0
50	105.1	73	8	448.44	3.39	2	8	0
51	81.3	81	8	423.43	3.56	2	7	0
1*	81.3	81	8	441.42	3.47	2	8	0
52	26.7	100	5	382.45	4.00	1	4	0
53	72.5	84	6	409.45	4.31	1	5	0
54	72.5	84	6	409.45	4.27	1	5	0
55	26.7	100	6	432.45	4.64	1	6	0
56	26.7	100	7	454.58	5.37	1	4	1
2*	26.7	100	6	432.45	4.77	1	6	0
3*	72.5	84	7	477.45	4.51	1	8	0
4*	72.5	84	7	477.45	4.58	1	8	0
57	26.7	100	7	404.52	4.56	1	4	0
58	26.7	100	7	465.43	4.98	1	3	0
59	26.7	100	7	420.97	4.96	1	3	0
60	26.7	100	7	438.96	5.05	1	4	1
61	26.7	100	7	422.51	4.66	1	5	0
62	45.2	93	7	430.54	3.97	1	5	0
63	53.0	91	9	444.57	4.17	1	5	0
64	35.9	97	6	394.48	4.03	1	4	0

65	32.7	98	6	391.48	4.91	1	4	0
66	35.9	97	6	344.42	3.03	1	4	0
67	32.7	98	6	341.42	3.86	1	4	0
68	26.7	100	6	382.40	3.86	1	6	0
69	45.2	93	7	356.46	3.02	1	4	0
5*	35.9	97	6	326.43	3.05	1	3	0
6*	35.9	97	7	402.53	4.55	1	3	0
7*	35.9	97	6	376.49	4.12	1	3	0
70	59.3	89	6	482.39	4.91	2	4	0
71	59.3	89	6	437.94	4.92	2	4	0
72	59.3	89	7	471.49	4.60	2	7	0
73	61.5	88	7	461.49	4.25	3	6	0
8*	81.3	81	8	491.48	4.39	2	8	0
[i]CQ	28.2	99	8	319.87	5.28	1	2	1
[j]PQ	60.2	88	6	259.35	2.76	2	3	0

[a]TPSA: topological polar surface area; [b]%ABS: human intestinal absorption, calculated by: %ABS=109-(0.345 x TPSA); [c]n-ROTB: number of rotatable bonds; [d]MW: Molecular weight (expressed as Dalton); [e]ALOGPs 2.1 (LogP): logarithm of compound partition coefficient between n-octanol and water; [f]n-OHNH: number of hydrogen bond donors; [g]n-ON: number of hydrogen bond acceptors; [h]LV, Lipinski`s violations; [i]CQ, chloroquine; [j]PQ, primaquine. *Previously synthesized by our group [10, 13, 14, 19]

2.6. Genotoxicity assay

As in previous studies with APD [10], the DNA-damaging effect or genotoxicity of the most representative compounds in their chemical structure and antiplasmodial activity was evaluated. Consequently, the preliminary genotoxicity screening SOS/umu test was performed because of the high degree of agreement between the SOS/umu test and the standardized Ames test (OECD guideline 471) [28, 29]. Positive and negative controls were correct for all the SOS/umu tests carried out. The new APD **37**-**39**, **47**, **52**-**61**, **64**-**68** and **70**-**73** were not considered genotoxic since the induction factor (IF) was always lower than 2 at non-cytotoxic concentrations, with or without the S9 fraction (Supplementary Table 1). It should be noted that the SOS/umu test allowed us to select the best candidates (screening purposes) from a toxicological point of view, and the results should be further evaluated with the standardized Ames test for regulatory purposes.

2.7. *In vivo* antimalarial activity

Taking into account the extensive SAR studies and toxicological profiles and in accordance with our protocols, the *in vivo* antimalarial activity in the *P. berghei* mouse model was evaluated following oral administration. The criteria to select compounds was based on the 3D7 IC_{50} (0.07 µM ≤ IC_{50} ≤ 7.3 µM) and FCR-3 IC_{50} values (0.07 µM ≤ IC_{50} ≤ 1.32 µM), SI > 50, appropriate *in silico* bioavailability, and a negative genotoxicity test. Therefore, the parasitemia reduction and mean survival days (MSD) for chloroquine, the sample vehicle (DMSO-water solution) and promising APD (**55**, **56**, **57**, **61**, **64**, **66**, **67**, and **70**-**73**) were evaluated at a unique oral dose (50 mg/kg x 4 days) (Figure 5 and Supplementary Table 2). The classic antimalarial drug chloroquine (CQ), or the positive group, showed a parasitemia reduction of 88.5 ± 9.6% (MSD = 11). This value is representative of five independent experiments and served as an indicator to verify if the test meets the required specifications. Compounds **66** and **72** exhibited significant parasitemia reductions of 96.4 ± 1.9% (MSD = 12) and 80.4 ± 6.7% (MSD = 10), respectively. Compounds **64**, **67**, **70**, and **71** showed parasitemia reductions superior to those of the control group (DMSO-water solution; ANOVA–Tukey test), but not higher than 50%. Despite their antiplasmodial activities (3D7 IC_{50} ≤ 1 µM and FCR-3 IC_{50} ≤ 0.6 µM), compounds **55**, **56**, **57**, and **61** did not display parasitemia reductions significantly superior to the control group (ANOVA–Tukey test). *In vivo* parasitemia reduction could not be evaluated for compound **73** due to the death of mice on the third day of the experiment (Supplementary Table 2).

We believe that parasitemia reduction values for newly synthesized APD **66** and **72** (96.4% and 80.4%, respectively) and the previous related compound **8*** (96.4% parasitemia reduction) [10] satisfactorily support the idea of APD as promising candidates for future ADME optimization programs.

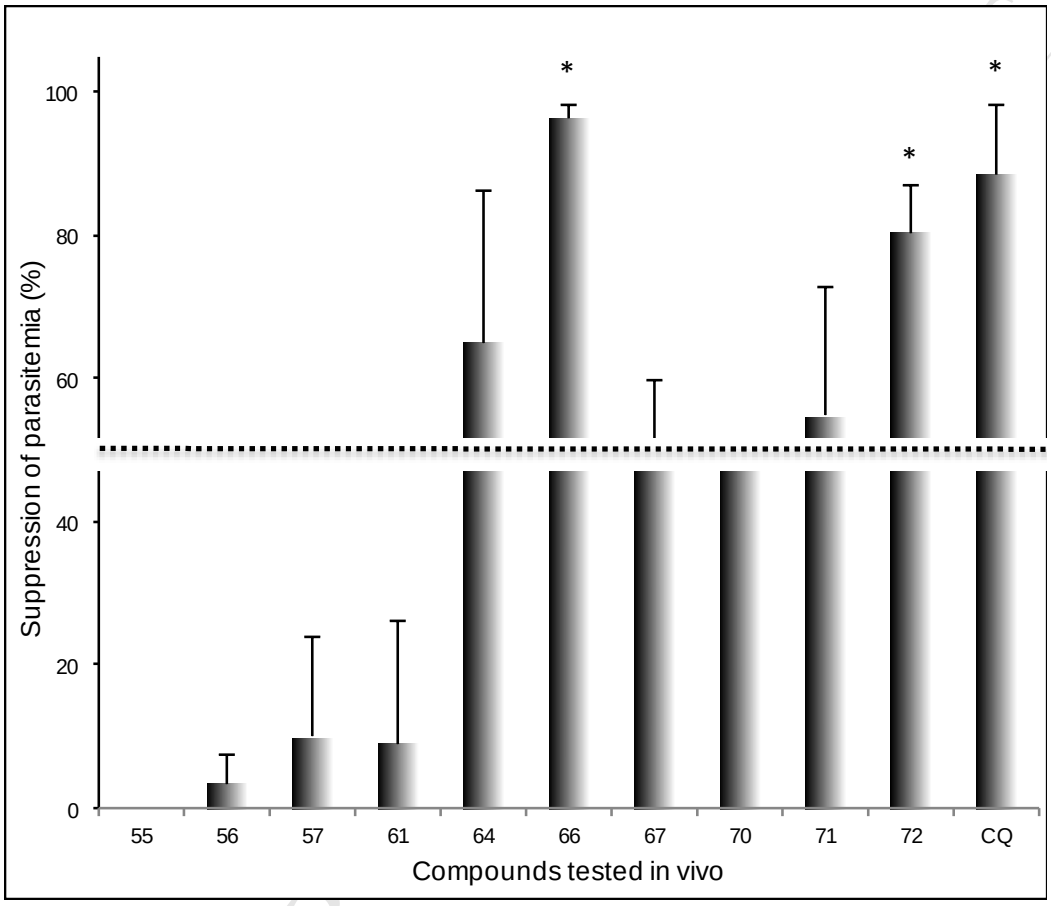

Figure 5. *In vivo* antimalarial efficacy data of selected APD in *P. berghei*-infected mice. *Percentage of inhibition significantly superior than 50% (Student t test).

2.8. Liver stage activity and sporogony inhibition

The ability of APD to act as dual- or triple-action antimalarials was determined by evaluating their human hepatocellular cytotoxicity, liver stage activity, and sporogony inhibition (Table 10 and Figure 6, respectively). Primaquine (PQ) was used as a reference drug in cytotoxicity and liver stage experiments for comparison. Based on their potent antiplasmodial activity against the FCR-3 strain (blood stage) and structural

diversity, twelve APD (**39**, **47**, **55**, **56, 61**, **64**, **65**, **66**, **71**, **72**, **1***, and **8***) were tested against exoerythrocytic forms (EEFs) of *P. berghei* (Table 10). Compounds **56**, **71**, **72**, **1***, and **8*** were considered active (IC_{50} values < 19 µM), with the most active being **71** and **72** (IC_{50} values ≤ 3.41 µM). It must be highlighted that compounds **71** and **72** exhibited slightly higher activities than PQ (IC_{50} = 3.65 µM). Only APD considered active against the *P. berghei* liver stage were tested against the EEFs of *P. falciparum* in a primary culture of human hepatocytes. As a result, only compounds **1*** and **8*** were active (IC_{50} < 1.8 µM), displaying *P. falciparum* liver-stage activity values that were not superior to that of the reference drug (IC_{50} = 0.4 µM).

To determine their selectivities, all these compounds were evaluated for mammalian cytotoxicity against different cell lines (HepG-2 and human's hepatocytes). As shown in Table 10, the selected compounds displayed SI values between 0.5 and 3.7 against the liver stage of *P. berghei* and ranging from 7.3 and 11.4 against *P. falciparum*, much lower than those obtained for the reference drug, PQ.

Based on their activity and selectivity index against the EEFs of *P. falciparum*, compounds **1*** and **8*** were tested for their ability to inhibit oocyst formation (Figure 6). *Anopheles stephensi* (*A. stephensi*) mosquitoes were allowed to feed on *P. berghei* GFP-infected mice 1.5 h after treatment with APD **1*** and **8*** (test group). The mosquito midguts were evaluated for two parameters, the presence of oocysts and the number of oocysts per mosquito compared to the control mosquito group. Compound **1*** reduced by 24% the infection of *A. stephensi* and by 70% the mean number of oocystes ($p < 0.001$) in comparison with the control group. Compound **8*** was toxic to mice at the concentration tested. These results offer crucial evidence of APD being able to act as triple-stage antimalarial compounds (blood, liver, and mosquito stages). Our results are

in agreement with related studies on classic arylamino alcohols, where the ability to act in different stages of the parasite had been reported [30].

Table 10. *In vitro* activity against human hepatocellular cells and *P. berghei* and *P. falciparum* liver stages.

Compound	Liver stage IC_{50} (μM)[a]		Cytotoxicity CC_{50} (μM)[b]		Liver stage SI[c,d]		Blood stage IC_{50} (μM)[a]
	P. berghei	*P. falciparum*	HepG-2[e]	Human[f]	*P. berghei*	*P. falciparum*	*P. falciparum (FCR-3)*
39	NA[g]	ND[h]	164.88 ± 23.10	ND			1.70 ± 0.20
47	NA	ND	253.23 ± 10.90	ND			2.88 ± 0.10
55	NA	ND	27.52 ± 0.60	ND			0.15 ± 0.03
56	5.42 ± 0.89	NA	19.90 ± 2.70	ND	3.7		0.33 ± 0.04
61	NA	ND	54.27 ± 6.90	ND			0.37 ± 0.02
64	NA	ND	30.37 ± 5.40	ND			0.22 ± 0.02
65	NA	ND	17.69 ± 3.10	ND			1.30 ± 0.20
66	NA	ND	19.54 ± 0.02	ND			0.19 ± 0.10
71	3.41 ± 0.59	NA	7.95 ± 1.20	ND	2.3		0.09 ± 0.06
72	2.7 ± 0.70	NA	6.22 ± 0.60	ND	2.3		0.08 ± 0.03
1*	18.24 ± 1.40	1.71 ± 0.99	10.40 ± 1.60	19.49 ± 2.94	0.6	11.4	0.48 ± 0.04
8*	12.08 ± 1.0	1.79	5.70 ± 1.80	13.08 ± 1.20	0.5	7.3	0.15 ± 0.01
PQ[i]	3.65 ± 0.50	0.4 ± 0.19	120 ± 5.70	54 ± 1.23	32.9	135	1.18 ± 0.71

Mean values of two independent experiments performed in triplicate ± standard deviation. [a]IC_{50}: Concentration that produces 50% of the inhibitory effect. [b]CC_{50}: Concentration that produces 50% of cytotoxicity. [c]SI: Selectivity index = CC_{50} HepG-2 cells/ Liver stage FCR-3 IC_{50} *P. berghei*. [d]SI: Selectivity index = CC_{50} Human cells/ Liver stage FCR-3 IC_{50} *P. falciparum*. [e]HepG-2: Human hepatocellular carcinoma cells. [f]Human: Primary human hepatocytes. [g]NA: Not active. [h]ND: Not determined. [i]PQ: Primaquine. [*]Previously synthesized by our group [10]

Figure 6. Compound **1*** reduce the number of oocysts in midgut of *A. stephensi*. Number of oocysts of *Pb*GFP in midgut of *A. stephensi* (n = 60 per group) was quantific using fluorescence microscopy. (A) Scatter dot plot showed number of oocyst per mosquito; black line represents median with interquartile range; (B) Bars plot showed mean of number of oocysts per group of treatment. Data are expressed as mean ± SD *** $p<0.001$

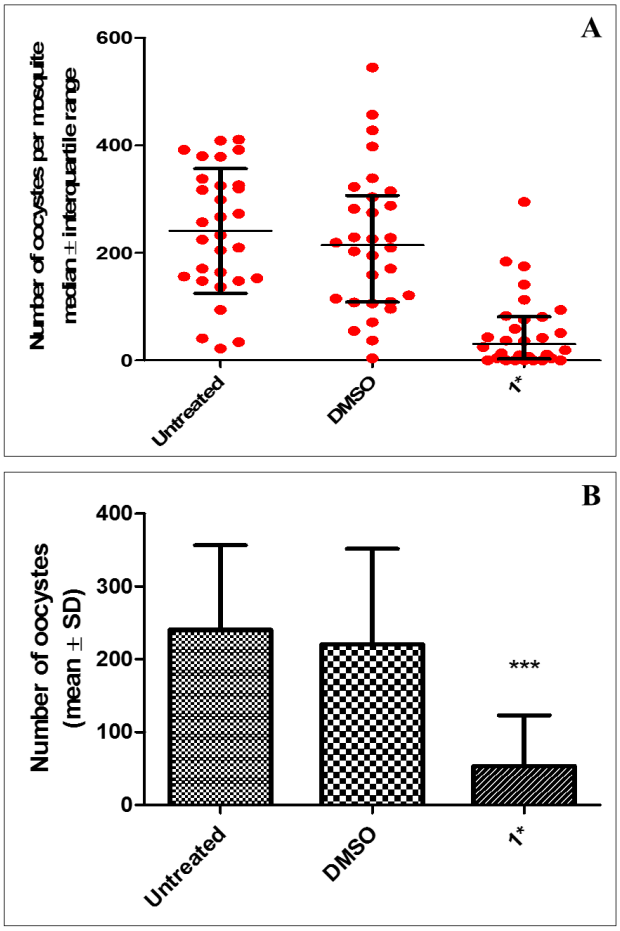

2.8. Target exploration of the *P. falciparum* Hsp90 chaperone

In our continuous search to understand the mechanism of action of APD, the hemozoin inhibition pathway and plasmepsin II enzyme were explored by our group previously; however, both were discarded as primary targets for APD [10]. Recently, the capacity to inhibit the Hsp90 of *P. falciparum* (*Pf*Hsp90) by amino alcohol-carbazoles had been reported in the literature [11]. The function of Hsp90 and other related compounds is to assist essential parasite proteins reaching their active conformations. Due to the nature of their protein substrates, called client proteins, the Hsp90 chaperone function is indispensable for the survival of the malaria parasite [31, 32], and inhibition of the chaperone is lethal to the parasite [33-36]. To validate the potential of the *Pf*Hsp90 chaperone as the target of the APD (**55**, **56**, **64**, **66**, **70-72**, **1***, and **8***), recombinant

*Pf*Hsp90 and *Pf*GRP94 nucleotide-binding domains were used to characterize the interaction of the selected compounds with the chaperone proteins using two independent methods, differential scanning fluorimetry (DSF) and surface plasmon resonance (SPR) analysis. Adenosine triphosphate (ATP), adenosine diphosphate (ADP), and compounds **5E** and **5B,** referenced in the literature as *Pf*Hsp90 inhibitors, were used as positive controls [11] (Supplementary Figure 1). Initially, their binding was determined using a DSF assay. In this assay, an interaction between the chaperone and a compound was measured as a change in the protein's melting temperature (T_m) by subtracting the T_m of the protein by itself to the melting value of the protein in the presence of the compound. Differences above or below 1 ˚C between the melting temperatures (ΔT_m) were considered indicative of a protein-compound interaction. As expected, the *Plasmodium* Hsp90 and GRP94 chaperones interacted with both ATP and ADP, but no change in the T_m was observed in the presence of any of the APD evaluated. To further exclude low-affinity interactions between the tested APD and the chaperones, their interaction was also evaluated by SPR. As was the case with the DSF assay, no binding events were recorded for the derivatives evaluated, but affinity constants in the expected range were obtained for the positive controls (**5E** K_d PfHsp90 = 0.007 µM, K_d PfGRP94 = 4480 µM and **5B** K_d PfHsp90 = 0.027 µM, K_d PfGRP94 = 0.017 µM). Therefore, the results from two independent methods failed to uncover any interaction between the APD and the malaria Hsp90 protein chaperone. These results would suggest that this protein is not the target for APD.

In general, our data reinforce our hypothesis that the APD could exhibit a mechanism of action different from the classic and other types of amino alcohols, and therefore APD can be considered candidates in future antimalarial drug optimization campaigns. Due to the appearance in recent years of drug-resistant strains for the first-line treatments

(ACTs) [4, 37], the development of antimalarial drugs with novel mechanisms of action is of crucial importance.

2.9. Immunoliposomes as a targeted drug delivery approach for APD

2.9.1. Selection of the APD to be assayed in immunoliposomes (iLPs) for targeted drug delivery approaches

The selection of APD for delivery approaches based on iLPs targeted to red blood cells (RBCs) was performed according to previously described protocols, compound solubility into liposome (LP) particles, and their absorption in the UV-visible range [38]. Compounds **55-68** exhibited poor solubility, rapidly precipitating once dissolved into the initial LP lipid mixture (250 µM drug for 10 mM total lipid) and being barely detectable above 300 nm. Due to the improved solubility of **72** and its absorption at 320 nm (Figure 7), this compound was selected for subsequent drug delivery assays into *P. falciparum* cultures.

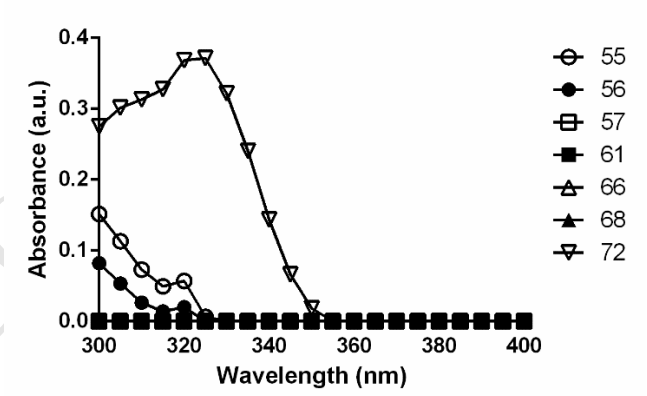

Figure 7. UV-visible determination of selected APD following LP encapsulation, removal of unencapsulated material and subsequent extraction of drug-containing LPs with 1% w/v SDS in RPMI-A, which was also used as a blank sample for absorbance subtraction.

*2.9.2. Characterization of the active encapsulation of **72** in LPs*

As observed with the analogue **8*** encapsulated through an identical protocol, **72** caused a significant LP surface charge alteration in the presence of the citrate buffer solution (pH 4.0) used for lipid film hydration (8.54 mV for **72** LPs vs. -2.73 mV for drug-free control particles of identical lipid compositions, Table 11).

Table 11. Interaction of **72** with LPs and stable encapsulation into the inner layer of LPs (500 µM drug for 10 mM lipid).

	Mean ζ-potential (mV) ± SD	
	LPs in citrate	**LPs after BE**
Control	-2.73 ± 0.26	-16.48 ± 2.35
72	8.54 ± 0.31	-18.2 ± 0.26

This charge perturbation disappeared after an external buffer exchange with phosphate-buffered saline (PBS) (pH 7.4), indicating the preferential accumulation of **72** in the inner membrane leaflet of the LPs. The light scattering-determined final LP size in PBS was 182.3 ± 1.65 nm, with a low polydispersity index of 0.16 ± 0.02. Whereas > 75% of **72** was incorporated in the LPs after the buffer exchange step, ~100% of this liposomized drug remained encapsulated at the end of the process, indicating a stable drug internalization (Table 12).

Table 12. Analysis of active drug encapsulation into LPs through a citrate/phosphate-buffered pH gradient. The compound concentration was determined by UV/vis spectroscopy after each step of the process, including (i) initial LP formation in citrate buffer (LPs citrate; here the highly lipophilic compound **72** was incorporated), (ii)

buffer exchange (BE) with PBS (LPs post-BE; here, CQ was added to the preformed LPs), and (iii) the ultracentrifugation of samples in PBS (LPs post-ultra), to determine the encapsulated drug at the end of the process. The volumes of all samples were kept equal for a straightforward reading of the drug concentrations, and the encapsulation efficiency (EE) was expressed as the percent of encapsulated drug vs. the total amount of drug in the sample.

	Drug (µM), mean ± SD	**EE (%), mean ± SD**
	72	
LPs citrate	232.3 ± 5.2	-
LPs post-BE	179.3 ± 3.9	77.2 ± 3.1
LPs post-ultra	181.8 ± 7.5	101.4 ± 5.6
	Chloroquine	
LPs post-BE + Drug	228.9 ± 5.0	-
LPs post-ultra	219.3 ± 4.7	95.8 ± 5.8

*2.9.3. P. falciparum growth inhibition assays with **72** actively encapsulated into iLPs targeted to glycophorin A (GPA)*

The potential of RBCs as drug carriers for future antimalarial therapies [38, 39] led us to explore the capacity of poorly soluble **72** for becoming internalized into RBCs. Non-significant differences in *P. falciparum* growth were observed for **72**-treated samples between washed and non-washed RBCs (with unretained drug being removed after 24 h incubation with RBCs and samples containing the full drug payload, respectively; Table 13), which confirmed the stable retention of the lipophilic **72** into RBCs. By contrast and in accordance with previous works [38], significant differences in *P. falciparum* growth were obtained for the water-soluble, doubly ionized drug CQ (i.e., p-values < 0.05 for washed vs. non-washed conditions).

Table 13. *P. falciparum* growth inhibition assays in parasite cultures at either ring (early) or late forms treated with **72** or CQ. The results are expressed as parasite growth IC_{50} (nM) after drug internalization into RBCs (washed RBCs) compared to non-washed RBC samples in which the excess antimalarials were not removed. The IC_{50} values were calculated considering the initially added drug concentrations. The corresponding washed vs. non-washed IC_{50}-fold change rates along with their related p-values calculated using log10(IC_{50}) values are included.

	IC50 (nM)			
	Washed RBCs	**Non-washed RBCs**	**Fold change**	***p* value**
		Rings		
72	513.5	181.3	2.8	0.40
[a]CQ	162.8	50.4	3.2	1.4×10^{-3}
		Late forms		
72	443.3	301.5	1.5	0.11
CQ	162.3	17.8	9.1	0.03

[a]CQ, chloroquine

The antimalarial performance of **72** after its active encapsulation into iLPs targeted to GPA (GPA-iLP[**72**] nanocarrier model) was subsequently assayed *in vitro* in *P. falciparum* cultures of the 3D7 strain exposed to the drug for only 15 min. When compared to the freely administered compound, immunoliposomal encapsulation provided a significant >5-fold improvement in drug the IC_{50} regardless of the moment in the parasite's life cycle when the drug was incorporated (i.e., early or late stage; Figure 8 and Table 14). This good performance of iLP-encapsulated **72** was obtained at drug concentrations where antibody-induced RBC agglutination is maintained at low levels (Figure 8). The previously mentioned enhancement in the **72** drug effectivity after GPA-iLP encapsulation was even superior when compared to CQ, utilized here as a control drug extensively used for malaria therapeutics. In this regard, GPA-iLP[CQ] only offered IC_{50} reductions in ca. ~3-fold units.

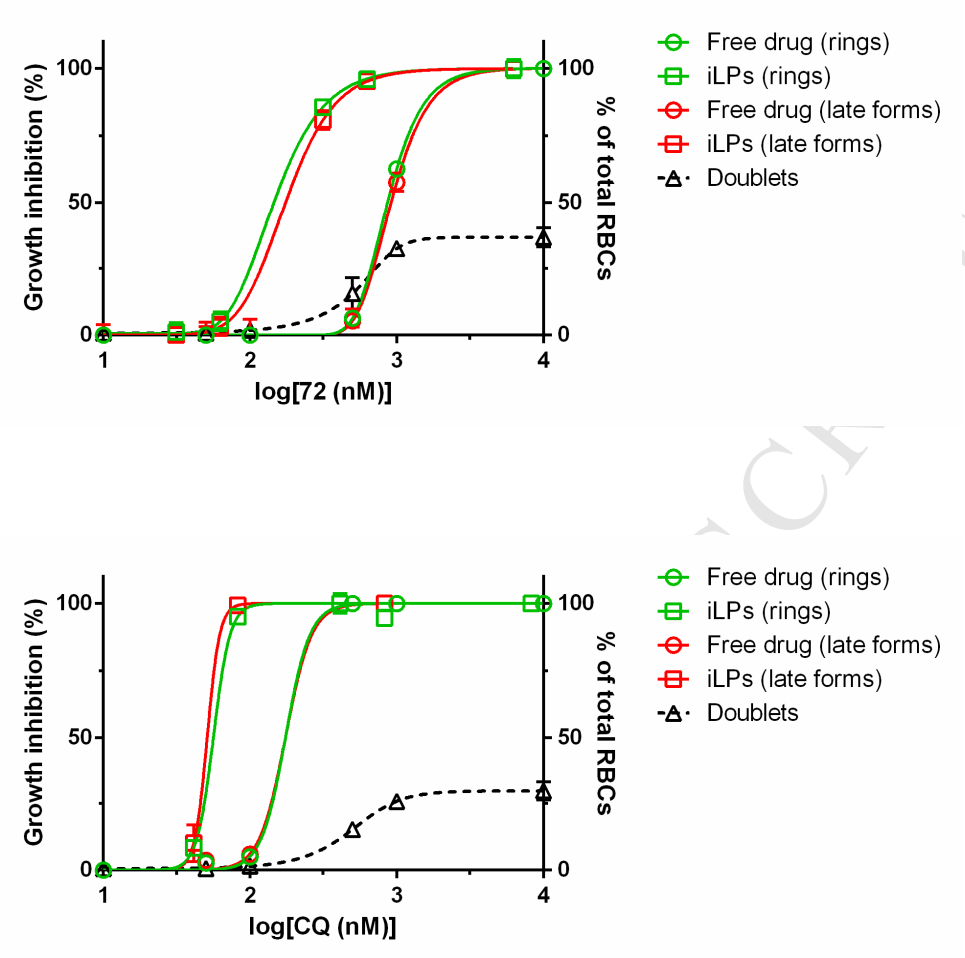

Figure 8. *In vitro P. falciparum* growth inhibition assays. GPA-iLP encapsulated vs. freely delivered **72** and CQ were added to parasite cultures at either ring or late stages and removed after 15 min; parasitemia was subsequently determined after 48 h of incubation. Agglutination rate (%) is expressed as the fraction of RBC doublets relative to the total amount of RBCs found in the sample.

Table 14. Data analysis of Figure 8. Results are expressed as parasite growth IC_{50} (nM) and the corresponding free drug vs. GPA-iLP[drug] IC_{50} fold change. Obtained p values were calculated using log10(IC_{50}) values.

	IC50 (nM)			
	Free drug	**GPA-iLP[drug]**	**Fold change**	***p* value**
		Rings		
72	867.0	146.2	5.9	$<1\times10^{-4}$
[a]CQ	174.5	56.3	3.1	9×10^{-4}
		Late forms		
72	916.2	174.6	5.2	$<1\times10^{-4}$
CQ	174.5	51.1	3.4	1×10^{-3}

[a]CQ, chloroquine

2.10. Separation, optical resolution, antiplasmodial activity, and cytotoxicity studies of APD enantiomers

2.10.1. Separation and optical resolution of APD enantiomers

To further determine the potential differences in antiplasmodial activity and cytotoxicity of the enantiomers of this work, supercritical fluid chromatography (SFC) was employed to optically resolve and isolate four representative active APD (compounds **55**, **66**, **72**, and **8***) into pure enantiomers. The pure enantiomers obtained from the preparative chromatography were studied using polarimetry, and the specific rotations measured are shown in Table 15.

Table 15. Specific rotatory power of each enantiomer

Compound	**Rotatory power**
55 F1	Levorotatory (-12.3)
55 F2	Dextrorotatory (+10.9)
66 F1	Levorotatory (-0.7)
66 F2	Dextrorotatory (+1.7)
72 F1	Levorotatory (-1.1)
72 F2	Dextrorotatory (+1.2)
8* F1	Levorotatory (-8.2)
8* F2	Dextrorotatory (+5.7)

*Previously synthesized by our group [10]

2.10.2. Antiplasmodial activity and cytotoxicity studies of APD enantiomers.

The *in vitro* antiplasmodial activity against a chloroquine-sensitive strain (3D7) and multidrug-resistant strain (FCR-3) of *P. falciparum* and the HepG-2 cytotoxicity of racemic APD and their individual enantiomers are shown in Table 16. From an antiplasmodial point of view, all the racemic mixtures were more active than their respective enantiomers, except for the (-)-isomer of compound **66** (3D7 strain). In the case of individual enantiomers, there was not found to be a clear tendency. For example, the (+)-isomers of compounds **55** and **8*** were more active than the (-)-isomers. In contrast, the (-)-isomers of compounds **66** and **72** were more active. Although, in our preliminary studies, no significant differences were found between the antiplasmodial activity of the APD enantiomers and racemic mixtures (chloroquine-sensitive F32 strain) [10], it is referenced in the literature that enantiomers of arylamino alcohols such as mefloquine or mefloquine derivatives sometimes did not exhibit a clear tendency with the same strain of *P. falciparum* [40]. From a cytotoxicity point of view, all the racemic mixtures were more selective than their respective enantiomers, except for the (+)-isomer of compound **8***, which was found to be 5 times more selective. Therefore, our collected data suggest that future campaigns to improve the cytotoxicity in APD by using a specific enantiomer is a viable strategy (e.g., **72**); however, further studies must be performed to define the absolute stereochemistry of the APD enantiomers.

Table 16. *In vitro* antimalarial activity against chloroquine sensitive strain (3D7) and multidrug-resistant strain (FCR-3) of *P. falciparum*, and HepG-2 cytotoxicity of racemic APD and their individual enantiomers.

Compound	IC_{50} (μM)[a] *P. falciparum*		CC_{50} (μM)[b]	SI[c]	CC_{50} (μM)[d]	SI[e]
	3D7	FCR-3	HepG-2[f]		HepG-2	

55	Racemic	0.16 ± 0.06	0.15 ± 0.03	27.52 ± 0.60	183	ND[g]	-
	(+)-Isomer	0,54 ± 0,06	0,21 ± 0,03	10,76 ± 2,42	51	36,12 ± 4,62	172
	(−)-Isomer	0,88 ± 0,1	0,20 ± 0,02	18,19 ± 0,6	91	61,51 ± 2,31	308
66	Racemic	7.31 ± 0.02	0.19 ± 0.10	19.54 ± 0.02	103	ND	-
	(+)-Isomer	28,73 ± 2,6	12,23 ± 1,92	96,01 ± 7,90	8	>145,17	>11.8
	(−)-Isomer	1,24 ± 0,12	0,66 ± 0,03	14,34 ± 2,51	22	>145,17	>219.9
72	Racemic	0.13 ± 0.01	0.08 ± 0.03	6.22 ± 0.60	78	ND	-
	(+)-Isomer	5,72 ± 0,18	0,65 ± 0,00	18,75 ± 4,26	29	79,85 ± 3,94	58
	(−)-Isomer	0,28 ± 0,14	0,39 ± 0,13	11,03 ± 3,19	28	27,80 ± 1,97	11
8*	Racemic	ND	0.15 ± 0.01	5.70 ± 1.80	38	ND	-
	(+)-Isomer	0,48 ± 0,06	0,19 ± 0,02	38,26 ± 1,00	201	37,64 ± 2,03	420
	(−)-Isomer	1,79 ± 0,02	0,87 ± 0,12	19,98 ± 2,22	23	4,13 ± 0,08	32

[a]IC_{50}: Concentration that produces 50% of the inhibitory effect.
[b]CC_{50}: Concentration that produces 50% of cytotoxicity at Universidad de Antioquia
[c]SI: Selectivity index = CC_{50} HepG-2 cells/ FCR-3 IC_{50} *P. falciparum* based on data from Universidad de Antioquia
[d]CC_{50}: Concentration that produces 50% of cytotoxicity at Université Toulouse
[e]SI: Selectivity index = CC_{50} HepG-2 cells/ FCR-3 IC_{50} *P. falciparum* based on data from Université Toulouse
[f]HepG-2: Human hepatocellular carcinoma cells
[g]ND: Not determined
*Previously synthesized by our group [10]

3. Conclusion

This manuscript has shown the design, synthesis, *in vitro* evaluation against chloroquine-sensitive (3D7 and D6) and multidrug-resistant (FCR-3 and C235) strains of *P. falciparum*, cytotoxicity studies (HepG-2 cells), *in silico* drug-likeness studies, genotoxicity profiles, *in vivo* efficacy in the *P. berghei* mouse model, liver-stage and sporogony inhibition studies, target exploration, targeted delivery using immunoliposomes, and enantiomer characterization (separation, optical resolution and biological profile) of new APD.

The design based on SARs (previous and new) and bioisostere replacements implemented in computational tools led to the identification of nine APD with promising *in vitro* (**55**, **56**, **61**, **64, 66**, and **70-73**) and *in vivo* (**66** and **72**) antimalarial profiles. Compounds **55**, **56**, **61**, **64**, **66** and **70-73** exhibited potent antiplasmodial activity against the chloroquine-resistant strain FCR-3 (IC_{50} < 0.28 µM), while compounds **55**, **56**, **64**, **70**, **71**, and **72** showed potent antimalarial activity against both chloroquine-sensitive and multidrug-resistant strains (IC_{50} < 0.7 µM for 3D7, D6, FCR-3 and C235). All of them share appropriate drug-likeness profiles, adequate selectivity indexes (77 < SI < 184), and an absence of genotoxicity in the SOS/umu screening test.

The *in vivo* efficacy in the *P. berghei* mouse model showed compounds **66** and **72** to be promising candidates, exhibiting significant parasitemia reductions of 96.4 % and 80.4 %, respectively. For the first time, the evidence of APD to act as triple-stage antimalarial compounds (blood, liver, and mosquito stages) had been reported, and this represents a feature that must be explored in depth in further studies. The target exploration of the *Pf*Hsp90 chaperone was performed to establish a possible mechanism of action; however, the protein was discarded as a primary target for APD. Immunoliposomes were used as a targeted drug delivery approach for APD to counteract its high lipophilic profile and low solubility in plasma. The antimalarial performance of APD **72** after its active encapsulation (GPA-iLP[**72**] nanocarrier model) showed a significant improvement in its antiplasmodial activity of more than five times compared to the freely administered compound. Antiplasmodial and cytotoxicity studies on racemic mixtures and individual enantiomers on APD emerge as a strategy for future campaigns of APD optimization. The use of the (+)-isomer for APD **8*** must be highlighted as a viable strategy to maintain the antiplasmodial activity (IC_{50} = 0.19 µM FCR-3) while improving at the same time the cytotoxicity ($201 \leq SI \leq 420$).

In summary, the new collected data strongly reinforce the hypothesis of APD as promising antimalarial compounds. Some facts that support this idea are (1) their easy synthetic accessibility; (2) their established and clear SARs; (3) their preliminary non-genotoxic profiles; (4) the agreement between the *in vitro* and *in vivo* studies (reaching nM values and high parasitemia inhibition, respectively); (5) their unknown mechanism of action that we found to differ from that of classical amino alcohols (e.g., hemozoin inhibition, plasmepsin II, and Hsp90), and (6) the viability of improving the antiplasmodial activity and cytotoxicity using strategies of drug design, drug delivery,

and enantiomeric separation. Further optimization of APD must be done through complementary SAR and pharmacokinetic (ADMET) studies.

4. Experimental section

4.1. Visualization and design software of new APD

The FieldTemplater™ module (in Forge™, 10.4.2, Cresset®, Litlington, Cambridgeshire, UK; http://www.cresset-group.com/forge/) and Spark™ software (10.4.0, Cresset®, Litlington, Cambridgeshire, UK; http://www.cresset-group.com/spark/) were used to visualize and generate bioactive confirmations and perform bioisosteric replacements on APD, respectively. Both software packages are based on Cresset's field technology that condenses the molecular fields of a molecule into a set of points around the molecule, called "field points." Thus, the electrostatic, van der Waals and hydrophobic potentials of the molecule can be represented as field points. These "field points" are generated using the eXtended Electron Distribution (XED) forcefield [21]. The four field types are represented as follows: red (electrophilic), blue (nucleophilic), orange (hydrophobic), and yellow (van der Waals attractive forces). The size of the field or spheres indicates whether more energetically favorable interactions can be made.

4.1.1. Exploration of Ar_2 region using a bioisostere replacement tool

The Spark™ workflow was applied to the previously reported antimalarial compound **8*** (starter compound); however, it is recommended that the moiety or group to be replaced be selected from the bioactive conformation of the starter compound. Due to the absence of crystallographic data for **8*** bound to its target, its bioactive conformation was calculated using the FieldTemplater™ module. The bioactive

conformation hunt by FieldTemplater™ is based on the hypothesis that two or more molecules that bind to a common active site tend to make similar conformations and interactions with the target. The most active antimalarial compounds previously reported by us (22-25*; *P. falciparum* FCR-3 IC50 ≤ 0.48 μM) were used as the set of ligands to perform the bioactive conformation hunt [10]. The compounds were drawn using ChemDraw Ultra software 7.0 (CambridgeSoft Ltd.), and the stereoisomerism was manually checked (R and S configurations). Two-dimensional (2D) structures were used as inputs for FieldTemplater™, and the protonation state was assigned according to Forge's built rules (pH = 7). A set of bioactive conformations were generated, and a final template was chosen based on the top scoring parameters such as similarity, field similarity, and volume similarity. Additionally, a visual inspection of the bioactive conformations was performed to ensure no anomalies in the alignments. The bioactive conformation *R* generated for compound **8*** was loaded in the Spark™ workflow, and the phenyl ring attached to the piperidine scaffold was selected for replacement (including substituents on the phenyl ring) (Table 1 and Figure 3). The type of bond formed in the results was not limited by the nature of the connecting atom (no constraints). The experiment was run using all the ZINC databases (commercial compounds) [22] that include "very common," "common," "less common," "rare," and "very rare." Finally, the 'Accurate but slow' conditions were left by default, especially the criteria to score the replacement fragments (50% field and 50% shape similarity).

4.2. Chemistry

4.2.1. Reagents and instruments

Chemical reagents and solvents were acquired from commercial sources and used as supplied. The synthesized and tested final compounds were chemically characterized by

infrared (IR), melting point (mp), proton nuclear magnetic resonance (^{1}H-NMR), and carbon nuclear magnetic resonance (^{13}C-NMR) spectra as well as by elemental microanalysis. Chemical reactions that utilize microwave irradiation were conducted using a CEM Discover S®-Class Microwave reactor, using continuous irradiation power from 0 to 200 W, and operating at a frequency of 50/60 Hz. Those reactions were performed in a 35 mL microwave vial sealed with a Teflon® crimp cap using 1,4-dioxane as solvent (Sigma-Aldrich). The reaction courses were monitored by thin-layer chromatography (TLC). An Alugram® SIL G/UV$_{254}$ (Layer: 0.2 mm) (Macherey-Nagel, Germany) was used for the TLC. Some final derivatives were purified by glass-column chromatography or automated flash chromatography with a binary gradient of dichloromethane (DCM) (synthesis grade SDS-Carlo Erba Reactifs, France) and methanol (MeOH) (Panreac Química S.A.) and UV variable dual-wavelength detection. The chromatography was developed using the CombiFlash® Rf (Teledyne Isco, Lincoln. USA) with DCM/MeOH as solvents and a normal phase of a 12 g Flash Column (RediSep® Rf Columns by Teledyne Isco, Inc., USA). IR spectra were recorded on a Nicolet Nexus FTIR (Thermo, Madison, WI, U.S.) in KBr pellets. Melting points were determined with a Mettler FP82 + FP80 apparatus (Greifensee, Switzerland). Elemental microanalyses were obtained on an Elemental Analyzer (LECO CHN-900, Michigan, USA) from vacuum-dried samples. The analytical results for C, H, and N were within ± 0.4 of the theoretical values. The final compounds were confirmed to have ≥96% purity, as determined by the elemental microanalysis results. The ^{1}H NMR and ^{13}C NMR spectra were recorded on a Bruker 400 Ultrashield (Rheinstetten, Germany) operating at 400 and 100 MHz, respectively, using tetramethylsilane (TMS) as the internal standard and dimethyl sulfoxide-*d6* (DMSO-*d6*) or chloroform ($CDCl_3$) as solvent. The NMR

spectra were processed using MestReNova 12®. The chemical shifts are reported in ppm (δ), and the coupling constant (J) values are given in Hertz (Hz).

4.2.2. General synthetic methods

*4.2.2.1. General method for the synthesis of protected aryl amines (**IIa-d**)*

A mixture of the protected 4-(*N*-Boc-amino)piperidine (1.2 equiv), the corresponding fluorinated derivatives (**Ia-d**) (1.0 equiv), K_2CO_3 (1.5 equiv) and acetonitrile (30 mL) was heated at reflux for 24 hours. The solvent was removed under reduced pressure, and the residue was dissolved in DCM (50 mL) and washed with water (3x30 mL). The organic phase was dried with anhydrous Na_2SO_4, filtered, and evaporated to dryness under reduced pressure. The residue was purified by gradient elution glass-column chromatography on silica gel using DCM/MeOH (v/v) as an eluent or gradient elution automated flash chromatography eluting with DCM/MeOH (v/v).

*4.2.2.1.1. [1-(2-bromo-4-cyanophenyl)-piperidin-4-yl]-carbamic acid tert-butyl ester (**IIa**)*. Yield; 67%, white solid, mp: 131.5-133.5°C. IR (KBr; cm^{-1}): *v* 3371 (s, υ_{N-H}), 3010 (w, $\upsilon_{C-H\ Ar}$), 2986 (m, υ_{C-H}), 2224 (s, υ_{CN}), 1686 (s, $\upsilon_{C=O}$), 1045 (m, υ_{C-Br}). ^{1}H NMR (400 MHz, $CDCl_3$): δ 7.81 (d, *J* = 1.9 Hz, 1H), 7.53 (dd, *J* = 8.3, 1.9 Hz, 1H), 7.04 (d, *J* = 8.4 Hz, 1H), 4.54 (s, 1H), 3.65 (s, 1H), 3.42 (d, *J* = 12.4 Hz, 2H), 2.82 (t, *J* = 11.7 Hz, 2H), 2.08 (dd, *J* = 13.4, 2.1 Hz, 2H), 1.64 (qd, *J* = 11.1, 3.7 Hz, 2H), 1.46 (s, 9H) ppm. ^{13}C NMR (100 MHz, $CDCl_3$): δ 155.29, 155.00, 137.46, 132.40, 121.12, 118.93, 117.98, 106.88, 79.64, 50.61 (2C), 47.51, 32.62 (2C), 28.53 (3C) ppm. Anal. cal. for $C_{17}H_{22}BrN_3O_2$: C, 53.69%; H, 5.83%; N, 11.05%; found: C, 53.30%; H, 5.75%; N, 10.88%.

*4.2.2.1.2. [1-(2-chloro-4-cyanophenyl)-piperidin-4-yl]-carbamic acid tert-butyl ester (**IIb**)*. Yield; 77%, white solid, mp: 129.5-130.5 °C. IR (KBr; cm^{-1}): *v* 3369 (m, υ_{N-H}),

3058 (w, $\upsilon_{C\text{-}H\ Ar}$), 2984 (m, $\upsilon_{C\text{-}H}$), 2224 (s, υ_{CN}), 1687 (s, $\upsilon_{C=O}$), 1044 (m, $\upsilon_{C\text{-}Cl}$). ^{1}H NMR (400 MHz, $CDCl_3$): δ 7.60 (d, *J* = 1.9 Hz, 1H), 7.48 (dd, *J* = 8.4, 1.9 Hz, 1H), 7.04 (d, *J* = 8.4 Hz, 1H), 4.57 (s, 1H), 3.64 (s, 1H), 3.45 (d, *J* = 12.4 Hz, 2H), 2.84 (td, *J* = 12.4, 2.0 Hz, 2H), 2.08 (d, *J* = 11.4 Hz, 2H), 1.69 – 1.56 (m, 2H), 1.46 (s, 9H). ^{13}C NMR (100 MHz, $CDCl_3$): δ 155.27, 153.62, 134.21, 131.77, 128.53, 120.73, 118.18, 106.04, 79.60, 50.12 (2C), 47.55, 32.63 (2C), 28.51 (3C). Anal. cal. for $C_{17}H_{22}ClN_3O_2$: C, 60.80%; H, 6.60%; N, 12.51%; found: C, 68.40%; H, 6.33%; N, 12.31%.

*4.2.2.1.3. [1-(4-cyano-2-trifluoromethyl-phenyl)-piperidin-4-yl]-carbamic acid tert-butyl ester (**IIc**).* Yield; 48%, white solid, mp: 153.5-154.5 °C, IR (KBr; cm^{-1}): *v* 3371 (s, $\upsilon_{N\text{-}H}$), 3085 (w, $\upsilon_{C\text{-}H\ Ar}$), 2975 (w, $\upsilon_{C\text{-}H}$), 2224 (m, υ_{CN}), 1701 (s, $\upsilon_{C=O}$), 1143 (m, $\upsilon_{C\text{-}F}$). ^{1}H NMR (400 MHz, DMSO-d_6) δ 8.12 (s, 1H), 8.03 (d, *J* = 8.4 Hz, 1H), 7.54 (d, *J* = 8.5 Hz, 1H), 6.90 (d, *J* = 6.9 Hz, 1H), 3.42 (s, 1H), 3.13 (d, *J* = 11.6 Hz, 2H), 2.86 (t, *J* = 11.4 Hz, 2H), 1.81 (d, *J* = 11.8 Hz, 2H), 1.52 (q, *J* = 11.0 Hz, 2H), 1.38 (s, 9H). ^{13}C NMR (100 MHz, DMSO-d_6): δ 155.94, 154.91, 137.17, 132.18 (q, $^{3}J_{CF}$ = 5.6 Hz), 124.19, 123.89 (q, $^{2}J_{CF}$ = 29.3 Hz), 123.30 (q, $^{1}J_{CF}$ = 273.8 Hz), 117.91, 105.63, 77.56, 51.79 (2C), 46.77, 31.92 (2C), 28.25 (3C). Anal. cal. for $C_{18}H_{22}F_3N_3O_2$: C, 58.53%; H, 6.00%; N, 11.38%; found: C, 58.22%; H, 6.06%; N, 11.32%.

*4.2.2.2. General method for the deprotection of amines (**IIIa-d**)*

The protected amine (**IIa-d**) was dissolved in 40 mL of a solution of HCl/AcOH (1:1) with stirring for 2 hours at room temperature. The solvent was removed under reduced pressure and the compound was dissolved in water. The aqueous solution was basified with NaOH 2M to basic pH and stirred for 1 hour, and then the product was extracted with DCM. The organic phase was dried with anhydrous Na_2SO_4 and filtered. After evaporating to dryness under reduced pressure, the crude product was purified by gradient elution glass-column chromatography on silica gel using DCM/MeOH (v/v) as

an eluent or gradient elution automated flash chromatography eluting with DCM/MeOH (v/v) to afford the desired deprotected amine (**IIIa-d**).

*4.2.2.2.1. 4-(4-amino-piperidin-1-yl)-3-bromobenzonitrile (**IIIa**).* Yield; 77%, white solid, mp: 75-76°C. IR (KBr; cm^{-1}): *v* 3354 (m, υ_{N-H}), 2935 (m, υ_{C-H}), 2224 (s, υ_{CN}), 1041 (w, υ_{C-Br}). ^{1}H NMR (400 MHz, DMSO-d_6) δ 8.06 (d, *J* = 2.0 Hz, 1H), 7.76 (dd, *J* = 8.4, 2.0 Hz, 1H), 7.21 (d, *J* = 8.5 Hz, 1H), 3.34 (d, *J* = 12.4 Hz, 2H), 2.80 – 2.67 (m, 3H), 1.81 (dd, *J* = 13.5, 2.6 Hz, 2H), 1.40 (ddd, *J* = 13.7, 11.1, 3.6 Hz, 2H). Anal. cal. for $C_{12}H_{14}BrN_3$: C, 51.44%; H, 5.04%; N, 15.00%; found: C, 51.04%; H, 5.10%; N, 14.61%.

*4.2.2.2.2. 4-(4-amino-piperidin-1-yl)-3-chlorobenzonitrile (**IIIb**).* Yield; 50%, white solid, mp: 89.6-90.6 °C. IR (KBr; cm^{-1}): *v* 3418, 3347 (m, υ_{N-H}), 3049 (w, $\upsilon_{C-H\ Ar}$), 2941 (s, υ_{C-H}), 2223 (s, υ_{CN}), 1059 (m, υ_{C-Cl}). ^{1}H NMR (400 MHz, DMSO-d_6): δ 7.89 (d, *J* = 2.0 Hz, 1H), 7.70 (dd, *J* = 8.5, 2.0 Hz, 1H), 7.20 (d, *J* = 8.5 Hz, 1H), 3.36 (d, *J* = 12.3 Hz, 2H), 2.79 – 2.70 (m, 3H), 1.80 (dd, *J* = 12.9, 2.9 Hz, 2H), 1.39 (td, *J* = 13.5, 3.6 Hz, 2H) ppm. ^{13}C NMR (100 MHz, DMSO-d_6): δ 153.67, 133.83, 132.26, 126.99, 121.18, 118.12, 104.41, 49.38 (2C), 47.63, 35.24 (2C) ppm. Anal. cal. for $C_{12}H_{14}ClN_3$: C, 61.15%; H, 5.99%; N, 17.83%; found: C, 61.02%; H, 6.29%; N, 18.16%.

*4.2.2.2.3. 4-(4-amino-piperidin-1-yl)-3-trifluoromethyl-benzonitrile (**IIIc**).* Yield; 16%, white solid, mp: 217-219 °C. IR (KBr; cm^{-1}): *v* 3361 (m, υ_{N-H}), 2935 (m, υ_{C-H}), 2228 (s, υ_{CN}), 1118 (m, υ_{C-F}). ^{1}H NMR (400 MHz, $CDCl_3$): δ 7.89 (s, 1H), 7.73 (d, *J* = 8.1 Hz, 1H), 7.30 (d, *J* = 8.5 Hz, 1H), 3.28 (d, *J* = 12.0 Hz, 2H), 3.01 – 2.90 (m, 1H), 2.86 (t, *J* = 11.2 Hz, 2H), 2.48 (bs, 2H), 1.98 (d, *J* = 11.4 Hz, 2H), 1.62 (td, *J* = 13.8, 3.4 Hz, 2H) ppm. ^{13}C NMR (100 MHz, $CDCl_3$): δ 156.18, 136.23, 132.39 (q, $^{3}J_{CF}$ = 5.5 Hz), 125.86 (q, $^{2}J_{CF}$ = 30.3 Hz), 123.44, 123.25 (q, $^{1}J_{CF}$ = 273.8 Hz), 118.05, 106.51, 52.11 (2C),

48.31, 35.30 (2C) ppm. Anal. cal. for $C_{13}H_{14}F_3N_3$: C, 57.99%; H, 5.24%; N, 15.61%; found: C, 57.60%; H, 5.50%; N, 15.24%.

*4.2.2.3. General method 1 for the synthesis of ketone derivatives (**1-36**)*

Ketones derivatives were prepared by Lehmann's method [41], which was adapted and optimized. In a 35 mL microwave vial, a solution of the corresponding substituted aryl methyl ketone (**V**) (1.0 equiv), the corresponding aryl amine as a base or hydrochloride salt (**IIIa-d**, **IVa-g**) (1.0 equiv), and paraformaldehyde (1.2 equiv) in 1,4-dioxane (4 mL) was stirred for 5 minutes at 20-22 °C. If necessary, concentrated HCl was added dropwise to the mixture until a pH of 1-2 was reached. The resulting mixture was heated using microwave irradiation at 100-110 °C, 20 psi, and 150 W for 5 minutes. Then, the mixture was poured into a flask and the 1,4-dioxane was removed *in vacuo*. The residue was diluted with H_2O (30 mL) and basified with 2M NaOH to basic pH and stirred for 1 hour. The mixture was transferred into a separatory funnel and extracted with DCM (3 × 50 mL). The organic phase was dried with anhydrous Na_2SO_4, filtered, and evaporated to dryness under reduced pressure. In some cases, the residue obtained was purified by gradient elution glass-column chromatography on silica gel using DCM/MeOH (v/v) as an eluent or gradient elution automated flash chromatography eluting with DCM/MeOH (v/v), affording the desired aryl-ketone (**1-36**). Based on our previous SAR studies [13, 14], the aryl-ketone derivatives were inactive against the NF54, 3D7, and FCR-3 strains of *P. falciparum*, and therefore they were not an objective or priority in the project.

*4.2.2.4. General method 2 for the synthesis of hydroxyl derivatives (**37-72**)*

To a pre-cooled suspension (0 °C) of the corresponding aryl-ketone residue (**1-36**) (1.0 equiv) in MeOH, sodium borohydride (3.0 equiv) was added over a period of 20-30 minutes. The solvent was removed under reduced pressure and the residue was

dissolved in DCM (50 mL) and then washed with water (3 x 30 mL). The organic phase was dried with anhydrous Na_2SO_4 and filtered. After evaporating the solvent to dryness under reduced pressure, the final compound was purified by gradient elution glass-column chromatography on silica gel using DCM/MeOH (v/v) as eluent or gradient elution automated flash chromatography eluting with DCM/MeOH (v/v). Selected compounds were converted to hydrochloride salts by adding a hydrogen chloride ethereal solution to the stirred compounds. Physical and spectroscopy data (IR, ^{1}H and ^{13}C NMR) for final APD are shown in the Supplementary material (NMR spectral data)

*4.2.2.5. Method for the synthesis of hydroxyl derivative (**73**)*

In a 100 mL flask, a pre-cooled suspension (0 °C) of the synthesized compound **VI** (1.0 equiv) in MeOH, hydrazine monohydrate (1.0 equiv) and Raney nickel (0.10 mL) were added over a period of 3 hours and filtered using celite. After evaporating the solvent to dryness under reduced pressure, the final compound was purified by gradient elution automated flash chromatography eluting with DCM/MeOH (v/v).

4.2.2.5.1. *3-[(1-(4-amino-2-trifluoromethylphenyl)piperidin-4-yl)amino]-1-(4-fluoronaphthalen-1-yl)propan-1-ol* (**73**). Yield; 60%, white solid, mp: 148-149 °C. IR (KBr; cm^{-1}): *v* 3359 (mb, υ_{O-H}), 2955 (m, υ_{C-H}), 1606 (w, $\upsilon_{C=C\ Ar}$), 1504 (s, $\upsilon_{C=C\ Ar}$), 1319 (s, υ_{C-F}). ^{1}H NMR (400 MHz, $CDCl_3$): δ 8.21 – 8.12 (m, 1H), 8.10 – 8.01 (m, 1H), 7.73 (ddd, *J* = 8.1, 5.6, 1 Hz, 1H), 7.62 – 7.51 (m, 2H), 7.19 (dd, *J* = 10.3, 8.1 Hz, 2H), 6.93 (d, *J* = 2.8 Hz, 1H), 6.81 (dd, *J* = 8.5, 2.8 Hz, 1H), 5.72 (dd, *J* = 8.3, 2.8 Hz, 1H), 3.73 (bs, 2H), 3.14 – 3.04 (m, 1H), 3.04 – 2.93 (m, 3H), 2.78 – 2.60 (m, 3H), 2.15 (ddt, *J* = 14.6, 5.9, 2.8 Hz, 1H), 2.06 – 1.96 (m, 2H), 1.88 (dddd, *J* = 14.6, 9.6, 8.2, 3.0 Hz, 1H), 1.67 – 1.51 (m, 2H) ppm. ^{13}C NMR (100 MHz, $CDCl_3$): δ 158.14 (d, *J* = 250.3 Hz), 143.96, 136.41 (d, *J* = 4.4 Hz), 136.39, 131.48 (d, *J* = 4.1 Hz), 128.54 (q, *J* = 28.1 Hz), 126.78, 125.68 (d, *J* = 1.9 Hz), 125.38, 124.10 (q, *J* = 273.4 Hz), 123.90 (d, *J* = 15.9

Hz), 123.12 (d, *J* = 2.8 Hz), 123.03 (d, *J* = 8.4 Hz), 121.42 (d, *J* = 5.9 Hz), 118.67, 113.11 (q, *J* = 5.5 Hz), 108.99 (d, *J* = 19.7 Hz), 72.47, 54.64, 53.11 (2C), 45.44, 36.60, 33.39 (2C) ppm. Anal. cal. for $C_{25}H_{27}F_4N_3O$: C, 65.06%; H, 5.9%; N, 9.11%; found: C, 65.24%; H, 5.53%; N, 8.92%.

4.3 Biology

4.3.1. In vitro antiplasmodial activity (3D7 and FCR-3 strains)

Compounds (**37-73**) were evaluated against the 3D7 chloroquine- sensible and FCR-3 multidrug-resistant strains of *P. falciparum* using the [^{3}H]-hypoxanthine (MP Biomedicals, USA) incorporation assay [42] with some modifications. A detailed description of the method can be found in our previous published article [10].

4.3.2. Cytotoxicity assay

The compound cytotoxicity (**37-73**) for the human hepatoma HepG2-A16 cell line (ATCC Hb-8065) was evaluated using the 3-(4,5-dimethylthiazol-2-yl)-2,5-diphenyltetrazolium bromide (MTT) viability assay [23]. A detailed description of the method can be found in our published previous article [43].

4.3.3. In vitro antiplasmodial activity (D6 and C235 strains)

Compounds **55, 56, 64-67, 70-72** were evaluated against the D6 chloroquine-sensitive and C235 multidrug-resistant strains of *P. falciparum* (obtained from the Walter Reed Army Institute of Research) using the Malaria SYBR Green-I Fluorescence (MSF) assay [44]. A detailed description of the method can be found in our previous published article [10].

4.3.4. In silico physicochemical property calculation and druglikeness evaluation

SwissADME (http://www.swissadme.ch/) [45] and Virtual Computational Chemistry Laboratory (http://www.vcclab.org/) [46] were used to calculate the Topological Polar Surface Area (TPSA), number of rotatable bonds, ALOGPs2.1, violations of Veber's rule [27], and violations of Lipinski's rule of five [26]. The human intestinal absorption (%ABS) was calculated using the Zhao's approach [25] :

$$\%\text{ABS} = 109 - (0.345 \times \text{TPSA})$$

4.3.5. Genotoxicity assay

The DNA-damaging effects of compounds **37**-**39**, **47**, **52**-**61**, **64**-**68** and **70**-**73** were studied using the SOS/umu test [47, 48]. A detailed description of the method can be found in our previous published article [10].

4.3.6. In vivo antimalarial activity

The classical 4-day suppressive or Peter's test was performed as follows [49, 50]. Swiss male mice weighing 20 ± 2 gr were infected intraperitoneally with 0.1 mL of saline solution (0.9%) containing 10^7 parasitized cells from *P. berghei* (ANKA strain) (day 0). Two hours after infection and at the same time during four consecutive days (from day 0 to 3), batches of five mice were orally treated at a dose of 50 mg/kg/day (drugs were dissolved in vehicle, water:DMSO). A control group received the vehicle, while a reference group was orally administered with chloroquine diphosphate at 3 mg/kg/day. The survival of the mice was verified daily, and the percentage of parasitized erythrocytes was determined on day 4 by the MSF assay with some modifications [51]. *In vivo* assays were conducted according to the DFUNC bioterium procedures and the Colombian guidelines on laboratory animal use and care (N°

008430). The test protocol was submitted to the Ethical Committee of Science Faculty at Universidad Nacional de Colombia.

4.3.7. Liver stage activity and sporogony inhibition

4.3.7.1. Parasites, cell lines and primary culture

P. berghei strain expressing green fluorescent protein (GFP) (*Pb*GPF) was used in the assays [52]. *Pb*GFP blood stage parasites were propagated in female Swiss mice (6–8 weeks old), *Anopheles stephensi* (*A. stephensi*) mosquitoes were fed on *Pb*GFP-infected mice and kept at 21 °C. *Pb*GFP sporozoites was freshly isolated from the salivary glands of infected mosquitoes 21 days post-feeding. *A. stephensi* mosquitoes infected with *P. falciparum* sporozoites (NF54 strain) were obtained from the Department of Medical Microbiology, University Medical Centre, St Radboud, Nijmegen, Netherlands. HepG2-A16 (ATCC HB-8065) was cultured in 96 well culture plate coated with rat tail collagen I (Becton-Dickinson, Le Pont de Claix, France) at 37 °C under 5% CO_2 in DMEM supplemented with 10% fetal calf serum and antibiotics (Life Technologies). Primary human hepatocytes were isolated and cultured as described previously [53].

4.3.7.2 In vitro liver stage development of P. berghei and P. falciparum

To assess liver stage development, HepG2-A16 cells (3×10^4 per well in collagen-coated 96-well plates) were infected with *Pb*GFP sporozoites (5×10^3 to 1×10^4 per well) and cultured for 40 h before analysis by fluorescence microscopy, after fixation with cold methanol and immunolabeling of EEFs with antibodies specific for *Plasmodium* Hsp70. Primary human hepatocytes (8×10^4 per well in collagen-coated 96-well plates) were infected with *P. falciparum* sporozoites (2.5×10^4 per well), and cultured for 8 days before fixation with cold methanol and immunolabeling of EEFs

with antibodies specific for *Plasmodium* Hsp70. Compounds were diluted in DMEM at 10 μg/mL as maximum concentration and seven serial dilution were done. The treatment of the cells was simultaneous to infection. The culture medium was changed 3 h and every 24 h post infection, and fresh compounds were added at the same concentration to maintain exposition. The cultures were allowed to grow at 37 °C in 5% CO_2. After time of development for each parasite, the cells were fixed with cold methanol, and then incubated for 1 h with antibody specific for *Plasmodium* Hsp70 at 37 ºC. The plates were washed three times with PBS, incubated with secondary antibody coupled to Alexa 594 (Life Technologies) for 1 hour at 37 ºC, using DAPI (Life Technologies) as a nuclei staining. Analysis of liver-stage parasites was performed using a CellInsight NXT HCS Platform (Thermo Scientific).

4.3.7.3 In vitro assay for determination of cytotoxicity in primary human hepatocytes. MTT assay.

Cytotoxicity evaluation of compounds using the primary human hepatocytes was evaluated by colorimetric test using 3-(4,5-dimethylthiazolyl-2)-2,5-diphenyltetrazolium bromide (MTT) [23]. In brief, the cells were cultured in a 96-well flat-bottomed plate (2×10^5 cells/well in 100 μL complete medium) and incubated for 24 h at 37 °C in a 5% CO_2 humidified atmosphere to allow monolayer formation. An aliquot of each compound dilution was then added to the wells in triplicate. The plates were incubated for another 48 h and then 30 μL MTT (2 mg/mL) was added and the plates were incubated again for 4 h; DMSO (96%, 130 μL) was added and plates incubated for a further 20 minutes at room temperature. The DMSO diluent agent and untreated cells in complete medium as negative controls were included. Absorbance was measured at 550 nm and statistical Prism software version 5.0 (GraphPad Software Inc.,

La Jolla, CA, USA) was used for calculating the concentration that produces 50% of cytotoxicity (CC_{50}).

4.3.7.4. P. berghei sporogonic assays

Two mice for experimental group were inoculated intraperitoneally with 200 µL of *Pb*GFP infected red blood cells (3000 parasites/µL). Four days post infection parasitaemia was monitored using Giemsa-stained blood smear and examined for the presence of gametocytes and testing for exflagellating gametocytes. *A. stephensi* mosquitoes were blood-feed from mice whose blood showed 1% of gametocytaemia during 1 hour. The compounds were administrated intraperitoneally at 100 mg/kg in DMSO 1.5 hours before infection of mosquitoes. Mice untreated and treated with DMSO (96%, 50 µL) were used as controls. After 8 days 30 mosquitoes per group were dissected. Midguts were removed and counted the number of oocystes by fluorescence microscopy. Inhibition of sporogony was calculated based on the oocyst numbers in the control mosquitoes considered as 100% infection. Statistical Prism software version 5.0 (GraphPad Software Inc., La Jolla, CA, USA) was used for comparison among groups.

4.3.8. Target exploration of the P. falciparum Hsp90 chaperone

4.3.8.1. Differential scanning fluorimetry (DSF)

DSF screening was carried out using a CFX96 Touch Real-Time PCR Detection System (BioRad, California). The *P. falciparum* nucleotide binding domains of Hsp90 and GRP94 were buffered in 25 mM HEPES pH 7.5, 250 mM NaCl and assayed in a 96-well format. The final concentration of the protein sample was optimized between 0.05 and 0.2 mg/mL for each protein. The concentration was optimized for each protein to avoid the saturation of the fluorescence detector. The compounds were evaluated at a

final concentration of 0.5 mM, and SYPRO Orange (Life Technologies, USA) was added as a fluorescence probe at a dilution of 1:1000. The experiments were conducted between 18 ˚C to 90 ˚C at a heating rate of 1 ˚C per minute, and the recorded fluorescence reads were fitted to the Boltzmann sigmoid function using DMAN software [54] . The inflection point of each fitted curve is defined as the melting temperature (T_m). The observed temperature shift, ΔT_m, was recorded as the difference between the T_m of the protein with ligand minus the T_m of the protein without ligand. Thermal shifts above or below 1˚C were considered significant.

4.3.8.2. Surface Plasmon Resonance (SPR) Analysis

SPR measurements were performed on a Biacore T200 instrument (GE Healthcare) at 25 ˚C. Purified *Pf*Hsp90 and *Pf*GRP94 nucleotide binding domains, as previously described [34], were immobilized on a CM5 sensor chip using NHS/EDC coupling following the manufacturer protocol to levels of 3000 and 7000 resonance units, respectively, and reference surfaces without immobilized proteins served as a control for nonspecific binding and refractive index changes. Seven different concentrations of the compounds between 0.4 nM and 1 mM were injected in triplicate over the sensor chip at 30µL/min in random order. The running buffer was 10 mM HEPES, pH 7.4, 150 mM NaCl, 0.005% P20, 1% DMSO and 2 mM $MgCl_2$. Buffer-only injections were used as blanks. All dissociation constants were estimated using double-subtracted sensorgrams using BiaEvaluation software (GE Healthcare). The relative responses recorded during the last 5 seconds of each injection were used to estimate the equilibrium response, and these values were used to estimate the dissociation constant (*Kd*). A steady-state affinity analysis was used as implemented in BiaEvaluation software.

4.3.9. Immunoliposomes as a targeted drug delivery approach for APD

4.3.9.1. Materials

Except where otherwise indicated, reagents were purchased from Merck & Co., Inc. (Kenilworth, NJ, USA), and reactions were performed at room temperature (22 to 24 °C). The lipids (all ≥99% purity according to the thin layer chromatography analysis) 1,2-distearoyl-sn-glycero-3-phosphocholines (DSPC), 1,2-distearoyl-*sn*-glycero-3-phosphoethanolamine-N-[maleimide(polyethylene glycol)-2000] (DSPE-PEG2000-Mal), and 1,2-dioleoyl-sn-glycero-3-phosphoethanolamine-N-[lissamine rhodamine B sulfonyl] (DOPE-Rho) were purchased dissolved in chloroform from Avanti Polar Lipids, Inc. (Alabaster, AL, USA). Mouse monoclonal IgG2b anti-human GPA (SM3141P) was purchased from Acris Antibodies GmbH (OriGene Company, Herford, Germany).

4.3.9.2. Preparation of liposomes (LPs) and active encapsulation of weakly basic compounds

LPs with the formulation DSPC:cholesterol:DSPE-PEG2000-Mal:DOPE-Rho, 84.5:10:5:0.5 were prepared by lipid film rehydration followed by sonication and the sizing of the multilamellar vesicles obtained through a 0.4 µm polycarbonate membrane extrusion, based on already established methods [55]. Chloroform was removed by rotary evaporation and the dried lipid film was later hydrated in PBS, supplemented with 10 mM ethylenediaminetetraacetic acid (EDTA) isotonic to Roswell Park Memorial Institute (RPMI) complete medium containing Albumax II (RPMI-A, Invitrogen). The sterility of the LP samples was maintained by rinsing all material in 70% ethanol and working in a laminar flow cabinet. The ζ-potential determination and dynamic light scattering size measurements were performed after a 1:30 sample dilution

in either deionized water (Milli-Q® system, Millipore) or PBS using a Zetasizer NanoZS90 (Malvern Ltd, Malvern, UK). Non-encapsulated material was removed by buffer exchange in 7-kDa Zeba™ spin desalting columns (Thermo Fisher Scientific, Inc.) using isotonic PBS. The encapsulation of the drugs was performed according to their hydrophilic nature. Lipophilic compounds already solubilized in organic solvents were directly added into the initial lipid mixture at a 1:40 or 1:10 drug:lipid ratio for *in vitro* and *in vivo* applications, respectively, whereas hydrophilic drugs were incorporated in the lipid hydrating buffer upon LP formation. The active encapsulation of drugs was performed upon the citrate-based pH gradient formation according to previously established protocols [38, 39].

4.3.9.3. Generation of immunoliposomes (iLPs)

The coupling to LPs of the monoclonal antibody (Ab) specific for the human erythroid-lineage-specific GPA membrane protein was performed as described elsewhere [38, 39, 56]. Briefly, Ab primary amines were derivatized with the sulfhydryl-containing crosslinking agent N-succinimidyl S-acetylthioacetate (SATA, Thermo Fisher Scientific, Inc.) at a 10× SATA/Ab molecular ratio and 0.5 mg Ab/mL for 10 mM maleimide-derivatized lipid conjugation conditions (i.e., thioether bond formation); these are optimized conditions defined in previous works [38]. Unconjugated Abs were removed by ultracentrifugation (150,000 g, 1 h, 4 °C), and pelleted GPA-iLPs were finally resuspended in isotonic PBS. Sterility was maintained throughout the coupling process by filtering all reagents through 0.22 μm pore size polyvinylidene difluoride filters (Millex-GV Syringe Filter Units, 4 mm, Millipore).

4.3.9.4. UV-visible spectral characterization of LP-encapsulated compounds

Encapsulated drugs were quantified as described elsewhere [38]. Briefly, LP samples were initially disrupted through the addition of 0.1 vol of 10% w/v sodium-dodecyl-sulphate (SDS), followed by 10 min bath sonication at 60 °C, and UV-spectra were retrieved from 2 µl of detergent-treated samples using an Epoch™ spectrophotometer (BioTek Instruments, Inc., Winooski, VT, USA). Drug standards for quantification were prepared in either RPMI-A plus 10 min water bath sonication at 60 °C or PBS depending on their lipophilic or hydrophilic nature, respectively. Empty SDS-treated LPs and drug solvents were used as blank controls for absorbance subtraction. Standard curves for drug quantification were finally obtained by linear/quadratic regression from at least three independent measurements.

4.3.9.5. Assessment of the antimalarial activity of drugs preloaded into non-infected erythrocytes

Blood group B human RBCs suspended at 6% hematocrit (v/v) in RPMI-A were diluted with one vol of 2× concentrated drugs in RPMI-A, and the mixture was incubated for 24 h at 37 °C. The drug-containing cells were subsequently spun down (700 *g*, 5 min) and taken up in fresh RPMI-A prior to the addition of *Plasmodium*-infected RBCs (pRBCs; resulting final parasitemia and hematocrit of 0.5% and 3.3%, respectively). Non-washed cells containing full drug dosages and similarly mixed with pRBCs were included for comparison. The parasite growth inhibition was finally assessed as described below.

4.3.9.6. Plasmodium falciparum in vitro culture and growth inhibition assays

The *P. falciparum* strain 3D7 was cultivated in blood group B human RBCs according to standard protocols [38, 39]. Synchronized cultures in the early ring stages (0-24 h post-invasion) were obtained by 5% sorbitol lysis [57]. Late-form trophozoite and schizont stages (24-36 h and 36-48 h post-invasion, respectively) were purified in 70% Percoll (GE Healthcare) [58]. Parasitemia was determined by the microscopic counting of blood smears fixed briefly with methanol and stained with Giemsa diluted 1:10 in Sorenson's buffer, pH 7.2, for 10 min. For culture maintenance, parasitemia was kept below 5% late forms, and 10% early forms by dilution with freshly washed RBCs and the medium was changed every 1-2 days. *P. falciparum in vitro* growth inhibition assays were conducted using synchronized cultures (>95%) in early or late form stages at 4% hematocrit and 1% parasitemia according to previously described protocols [38, 39]. Briefly, one culture volume of 2× concentrated drug solution in RPMI-A was added to the parasitized cell suspension, and the mixture was incubated under orbital stirring for 15 min in 2-ml Petri dishes. The cells were finally transferred to microcentrifuge tubes and spun down, replacing the medium with fresh RPMI-A. The resulting cell suspension was then seeded on 96-well plates and further incubated for a complete 48-h growth cycle under the conditions described above. For the determination of parasite growth inhibition, samples were diluted 1:100 in isotonic PBS, and the DNA of pRBCs (the only nucleated cells present in the culture) was stained by the addition of 0.1 μM Syto11 (Thermo Fisher Scientific, Inc.) in the final mixture before proceeding to the flow cytometry analysis. *Plasmodium* cultures were analyzed at 0.02% hematocrit in PBS with a BD LSRFortessa™ cell analyzer (Becton, Dickinson and Company, New Jersey, USA). Forward- and side-scatter areas (FSC-A, SSC-A) on a linear scale were used to gate the RBC population, and Syto11-stained pRBCs were detected by excitation through a 488 nm laser and emission collection with a 525/50 (Pacific Blue-

A) nm bandpass filter in a logarithmic scale. The acquisition was configured to stop after recording 20000 events within the RBC population. Parasitized erythrocytes in late forms were discerned from those in early stages, when required, using their increased Syto11 signal resulting from the presence of segmented parasites with multiple nuclei. Growth inhibition in drug-treated samples was defined as the percentage decrease in parasitemia within the second generation of parasites relative to the untreated control samples. RBC agglutinates were determined after incubation with iLPs by means of counting those cell disproportion events in FSC height-area (H-A) confronted parameters, which indicated the presence of cell doublets as previously described [56].

4.3.10. Separation, optical resolution, antiplasmodial activity, and cytotoxicity studies of APD enantiomers

4.3.9.10. Separation and optical resolution of APD enantiomers

Enantioseparation has emerged as an essential technique to be implemented in the pharmaceutical world [59]. Supercritical fluid chromatography (SFC) has become a mainstream technology for chiral separations based on its higher efficiency, throughput, and wide applicability. Superior and faster separations are obtained, resulting in improved resolution and reduced run time, sample and solvent [60]. The separation of enantiomers involves analytical-scale chiral chromatography followed by a preparative scale SFC chromatography. Analytical SFC studies were performed on an ACQUITY UltraPerformance Convergence Chromatography System™ (UPC^2)® from Waters coupled to a diode array detector and to a mass detector provided with an electrospray source and a simple quadrupole. The analyses were run on a Chiralpak IA-3 3 μm (4.6 x 100 mm) column eluted with supercritical CO_2 (channel A) and isopropanol (*i*-Pr) with 0.1% trifluoroacetic acid (TFA) and 0.1% diethylamine (DEA) (channel B) under

gradient conditions. The elution is carried out by a proportional gradient, the percentages of which are defined in the following table:

Table 17. Gradient of mobile phase for analytical SFC

	Time (min)	**Flow rate**	**%A[a]**	**%B[b]**
1	Initial	1.500	90.0	10.0
2	5.00	1.500	50.0	50.0
3	7.00	1.500	50.0	50.0
4	7.50	1.500	90.0	10.0

[a] %A= % supercritical CO_2 (channel A)
[b] %B= % *i*-Pr with 0.1% TFA and 0.1% DEA

The samples were diluted in 0.5 mL of MeOH and filtered with 0.2 μm autofiltration vials with polytetrafluoroethylene membranes. The analytical separations were run at 40 ºC with a flow rate of 1.5 mL/min and a pressure of 120 bar. The volume of the injection for all compounds was 10 μL and the total duration of the analysis was 10 min to allow the column to reequilibrate between each analysis. The detection was carried out with a PDA detector coupled to a simple quadrupole mass detector from Waters setting at 219 nm for compounds **55** and **72**, 213 nm for compound **8*** and 207 nm for compound **66**. The mass conditions were capillary voltage: 3.5 kV; cone tension: 30 V; extractor voltage: 3 V; Rf lens: 0.1 V; source temperature: 150 °C; desolvation temperature: 450 °C; nitrogen flow desolvation: 900 L/h; and cone nitrogen flow: 50 L/h D515 = 0.5 mL/min. The desired mass/charge (m/z) ranged from 150 to 650 daltons. Note: Each sample can be processed with all wavelengths between 190 and 600 nm.

Preparative scale chiral separations were run on the Prep 80q SFC System with a 2489 UV detector from Waters using a Chiralpak IA 5 μm (20 x 250 mm) column monitoring

at 219 nm for compounds **55** and **72**, 213 nm for compound **8*** and 207 nm for compound **66**. The crude products are diluted in *i*-Pr and filtered at 0.45 μM. All compounds were eluted in isocratic mode using a mixture of supercritical CO_2 and *i*-Pr supplemented with 0.1% TFA + 0.1% DEA at a flow rate of 40 mL/min and a pressure of 100 bar. The working temperature was 40 ºC, and the injection volume was 2 mL. The concentrations of the different injected solutions and the retention times of each enantiomer are summarized in the following table.

Table 18. Summary of retention times, concentration, co-solvent % and working wavelength for preparative separation of each product

Comp.	**RT (mn)**		**Concentration (mg/mL)**	**Co-solvent (%)**	**λ (nm)[c]**
	(Δ enantiomer)[a]	**(Λ enantiomer)[b]**			
55	4.3	6.4	10.4	25	219
66	18.5	20.5	8.43	15	207
72	11.3	14.5	3.975	20	219
8*	12.9	16.1	5.16	20	213

[a] Retention time of less retained enantiomer
[b] Retention time of more retained enantiomer
[c] Working wavelength

The purification of chiral compounds by SFC usually utilizes an isocratic method and stacked injections for optimal collection efficiency. To increase the productivity, the stacked injections provide the possibility of performing the second injection before the end of the elution of the second enantiomer. Postenantioseparation analysis was determined on an ACQUITY UPC^2 System from Waters with an UV detector coupled to a simple quadrupole mass detector from Waters. Purities very close to 100% were obtained in all cases. All of the analytical SFC files before and after the chiral resolution and the preparative SFC files of each compound are shown in the Supplementary Information (see Supplementary Data 1, 2 and 3). Finally, the measurement of the

rotatory power for the pure enantiomers was determined using polarimetry. For each analysis, 20 mg of each of the pure enantiomers diluted in 2 mL of MeOH were required. The rotatory power was measured at 589 nm on a P2000 polarimeter from Jasco at 20 °C. A series of ten measurements was carried out. The specific rotatory power was calculated according to Biot's law as follows:

$$[\alpha]_{589}^{20} = \frac{\alpha}{C.l}$$

Where:

• α: rotation potential or angle of rotation of the plane of polarization (deg);

• l: thickness of active substance crossed (dm);

• C: concentration of dissolved substance (g.cm-3);

•[α]T,λ: specific rotatory power

Acknowledgments

This work was supported by PIUNA Project (Universidad of Navarra), Foundation CAN (grant number 70391), Colciencias (grant number 111526934273; contract RC-597-2013), Ministerio de Economía y Competitividad (MINECO) of Spain (grant BIO2014-52872-R and FEDER funds), Generalitat de Catalunya (grant 2014-SGR-938) and the Instituto de Salud Tropical (ISTUN) of Universidad de Navarra. Miguel Quiliano is grateful to “Programa Nacional de Innovación para la competitividad y productividad” (Innóvate-Perú) for his Ph.D. scholarship (grant 065-FINCYT-BDE-2014). Ernest Moles is grateful to the subprograma de Formación de Personal Investigador of the MINECO for his scholarship. Leonardo Bonilla-Ramirez is funded by Colciencias Grants (grant 528–2011). Diego A. Nieto-Aco was supported by the Instituto General de Investigación of Universidad Nacional de Ingeniería and the

Research Experience for Peruvian Undergraduates (REPU) program. ISGlobal and IBEC are members of the CERCA Programme (Generalitat de Catalunya). We thank Cresset company for the academic licensing of Spark™ and Forge™. We thank Dr. Dominique Mazier of the group "Identification and Pre-Clinical Validation of Novel Therapeutic Targets against Malaria" at the Centre d'Immunologie et des Maladies Infectieuses-UPMC for the laboratory facilities to perform the transmission and hepatic phase tests. We thank the Integrated Screening Platform of Toulouse (PICT, IBISA) for the record of the analytical chromatograms using UPC^2. We thank the Institut de Chimie de Toulouse (ICT, FR2599) for the preparative chromatograms using Prep80.

Appendix A. Supplementary material

Supplementary information related to this article can be found at

References

[1] WHO, World malaria report 2017, Geneva, 2017.
[2] M.A. Phillips, J.N. Burrows, C. Manyando, R.H. van Huijsduijnen, W.C. Van Voorhis, T.N.C. Wells, Malaria, Nat. Rev. Dis. Primers, 3 (2017) 17050.
[3] K. Haldar, S. Bhattacharjee, I. Safeukui, Drug resistance in Plasmodium, Nat. Rev. Microbiol., 16 (2018) 156.
[4] K.M. Tun, M. Imwong, K.M. Lwin, A.A. Win, T.M. Hlaing, T. Hlaing, K. Lin, M.P. Kyaw, K. Plewes, M.A. Faiz, M. Dhorda, P.Y. Cheah, S. Pukrittayakamee, E.A. Ashley, T.J.C. Anderson, S. Nair, M. McDew-White, J.A. Flegg, E.P.M. Grist, P. Guerin, R.J. Maude, F. Smithuis, A.M. Dondorp, N.P.J. Day, F.ß. Nosten, N.J. White, C.J. Woodrow, Spread of artemisinin-resistant Plasmodium falciparum in Myanmar: a cross-sectional survey of the K13 molecular marker, Lancet Infect. Dis., 15 (2015) 415-421.
[5] Y.-L. Fan, X.-W. Cheng, J.-B. Wu, M. Liu, F.-Z. Zhang, Z. Xu, L.-S. Feng, Antiplasmodial and antimalarial activities of quinolone derivatives: An overview, Eur. J. Med. Chem., 146 (2018) 1-14.
[6] Y.-Q. Hu, C. Gao, S. Zhang, L. Xu, Z. Xu, L.-S. Feng, X. Wu, F. Zhao, Quinoline hybrids and their antiplasmodial and antimalarial activities, Eur. J. Med. Chem., 139 (2017) 22-47.
[7] K.T. Andrews, G. Fisher, T.S. Skinner-Adams, Drug repurposing and human parasitic protozoan diseases, Int. J. Parasitol. Drugs Drug Resist., 4 (2014) 95-111.
[8] M.A. Biamonte, Realistically, how far are we from a universal malaria drug?, Future Med. Chem., 6 (2014) 123-126.

[9] A.K. Bhattacharjee, J.M. Karle, Molecular Electronic Properties of a Series of 4-Quinolinecarbinolamines Define Antimalarial Activity Profile, J. Med. Chem., 39 (1996) 4622-4629.
[10] M. Quiliano, A. Mendoza, K.Y. Fong, A. Pabón, N.E. Goldfarb, I. Fabing, A. Vettorazzi, A. López de Cerain, B.M. Dunn, G. Garavito, D.W. Wright, E. Deharo, S. Pérez-Silanes, I. Aldana, S. Galiano, Exploring the scope of new arylamino alcohol derivatives: Synthesis, antimalarial evaluation, toxicological studies, and target exploration, Int. J. Parasitol. Drugs Drug Resist., 6 (2016) 184-198.
[11] T. Wang, P. Mäser, D. Picard, Inhibition of Plasmodium falciparum Hsp90 Contributes to the Antimalarial Activities of Aminoalcohol-carbazoles, J. Med. Chem., 59 (2016) 6344-6352.
[12] W. Wang, Q. Li, Y. Wei, J. Xue, X. Sun, Y. Yu, Z. Chen, S. Li, L. Duan, Novel carbazole aminoalcohols as inhibitors of β-hematin formation: Antiplasmodial and antischistosomal activities, Int. J. Parasitol. Drugs Drug Resist., 7 (2017) 191-199.
[13] A. Mendoza, S. Perez-Silanes, M. Quiliano, A. Pabon, S. Galiano, G. Gonzalez, G. Garavito, M. Zimic, A. Vaisberg, I. Aldana, A. Monge, E. Deharo, Aryl piperazine and pyrrolidine as antimalarial agents. Synthesis and investigation of structure-activity relationships, Exp. Parasitol., 128 (2011) 97-103.
[14] S. Perez-Silanes, L. Berrade, R. Garcia-Sanchez, A. Mendoza, S. Galiano, B. Perez-Solorzano, J. Nogal-Ruiz, A. Martinez-Fernandez, I. Aldana, A. Monge, New 1-Aryl-3-Substituted Propanol Derivatives as Antimalarial Agents, Molecules, 14 (2009) 4120.
[15] M. Quiliano, I. Aldana, Quinoxaline and Arylaminoalcohol Derivatives as Antiplasmodial and Leishmanicidal Agents: A Review of our First Ten Years in the Field, Rev. Virtual Quim., 5 (2013) 1120-1113.
[16] S.J. Burgess, J.X. Kelly, S. Shomloo, S. Wittlin, R. Brun, K. Liebmann, D.H. Peyton, Synthesis, Structure−Activity Relationship, and Mode-of-Action Studies of Antimalarial Reversed Chloroquine Compounds, J. Med. Chem., 53 (2010) 6477-6489.
[17] B. Gunsaru, S.J. Burgess, W. Morrill, J.X. Kelly, S. Shomloo, M.J. Smilkstein, K. Liebman, D.H. Peyton, Simplified Reversed Chloroquines To Overcome Malaria Resistance to Quinoline-Based Drugs, Antimicrob. Agents Chemother., 61 (2017) e01913-01916.
[18] D.J. Lowes, W.A. Guiguemde, M.C. Connelly, F. Zhu, M.S. Sigal, J.A. Clark, A.S. Lemoff, J.L. Derisi, E.B. Wilson, R.K. Guy, Optimization of Propafenone Analogues as Antimalarial Leads, J. Med. Chem., 54 (2011) 7477-7485.
[19] L. Orús, S. Pérez-Silanes, A.-M. Oficialdegui, J. Martínez-Esparza, J.-C. Del Castillo, M. Mourelle, T. Langer, S. Guccione, G. Donzella, E.M. Krovat, K. Poptodorov, B. Lasheras, S. Ballaz, I. Hervías, R. Tordera, J. Del Río, A. Monge, Synthesis and Molecular Modeling of New 1-Aryl-3-[4-arylpiperazin-1-yl]-1-propane Derivatives with High Affinity at the Serotonin Transporter and at 5-HT1A Receptors, J. Med. Chem., 45 (2002) 4128-4139.
[20] V. Purohit, A.K. Basu, Mutagenicity of Nitroaromatic Compounds, Chem. Res. Toxicol., 13 (2000) 673-692.
[21] T. Cheeseright, M. Mackey, S. Rose, A. Vinter, Molecular Field Extrema as Descriptors of Biological Activity: Definition and Validation, J. Chem. Inf. Model., 46 (2006) 665-676.
[22] J.J. Irwin, T. Sterling, M.M. Mysinger, E.S. Bolstad, R.G. Coleman, ZINC: A Free Tool to Discover Chemistry for Biology, J. Chem. Inf. Model., 52 (2012) 1757-1768.

[23] T. Mosmann, Rapid colorimetric assay for cellular growth and survival: Application to proliferation and cytotoxicity assays, J. Immunol. Methods, 65 (1983) 55-63.
[24] P. Ertl, B. Rohde, P. Selzer, Fast Calculation of Molecular Polar Surface Area as a Sum of Fragment-Based Contributions and Its Application to the Prediction of Drug Transport Properties, J. Med. Chem., 43 (2000) 3714-3717.
[25] Y. Zhao, M. Abraham, J. Le, A. Hersey, C. Luscombe, G. Beck, B. Sherborne, I. Cooper, Rate-Limited Steps of Human Oral Absorption and QSAR Studies, Pharm. Res., 19 (2002) 1446-1457.
[26] C.A. Lipinski, F. Lombardo, B.W. Dominy, P.J. Feeney, Experimental and computational approaches to estimate solubility and permeability in drug discovery and development settings, Adv. Drug Del. Rev., 23 (1997) 3-25.
[27] D.F. Veber, S.R. Johnson, H.-Y. Cheng, B.R. Smith, K.W. Ward, K.D. Kopple, Molecular Properties That Influence the Oral Bioavailability of Drug Candidates, J. Med. Chem., 45 (2002) 2615-2623.
[28] OECD, Test No. 471: Bacterial Reverse Mutation Test, OECD Publishing, 1997.
[29] G. Reifferscheid, J. Heil, Validation of the SOS/umu test using test results of 486 chemicals and comparison with the Ames test and carcinogenicity data, Mutat. Res.-Genet. Toxicol., 369 (1996) 129-145.
[30] M. Delves, D. Plouffe, C. Scheurer, S. Meister, S. Wittlin, E.A. Winzeler, R.E. Sinden, D. Leroy, The Activities of Current Antimalarial Drugs on the Life Cycle Stages of Plasmodium: A Comparative Study with Human and Rodent Parasites, PLoS Med., 9 (2012) e1001169.
[31] G. Banumathy, V. Singh, S.R. Pavithra, U. Tatu, Heat Shock Protein 90 Function Is Essential for Plasmodium falciparum Growth in Human Erythrocytes, J. Biol. Chem., 278 (2003) 18336-18345.
[32] S.R. Pavithra, R. Kumar, U. Tatu, Systems Analysis of Chaperone Networks in the Malarial Parasite Plasmodium falciparum, PLoS Comput. Biol., 3 (2007) e168.
[33] A.G. Bayih, D.R. Pillai, Mouse studies on inhibitors of Plasmodium falciparum Hsp90: progress and challenges, Parasitology, 141 (2014) 1216-1222.
[34] C. Murillo-Solano, C. Dong, C.G. Sanchez, J.C. Pizarro, Identification and characterization of the antiplasmodial activity of Hsp90 inhibitors, Malar. J., 16 (2017) 292.
[35] N. Roy, R.K. Nageshan, S. Ranade, U. Tatu, Heat shock protein 90 from neglected protozoan parasites, Biochim. Biophys. Acta, 1823 (2012) 707-711.
[36] T. Wang, W.H. Bisson, P. Mäser, L. Scapozza, D. Picard, Differences in Conformational Dynamics between Plasmodium falciparum and Human Hsp90 Orthologues Enable the Structure-Based Discovery of Pathogen-Selective Inhibitors, J. Med. Chem., 57 (2014) 2524-2535.
[37] E.A. Ashley, M. Dhorda, R.M. Fairhurst, C. Amaratunga, P. Lim, S. Suon, S. Sreng, J.M. Anderson, S. Mao, B. Sam, C. Sopha, C.M. Chuor, C. Nguon, S. Sovannaroth, S. Pukrittayakamee, P. Jittamala, K. Chotivanich, K. Chutasmit, C. Suchatsoonthorn, R. Runcharoen, T.T. Hien, N.T. Thuy-Nhien, N.V. Thanh, N.H. Phu, Y. Htut, K.-T. Han, K.H. Aye, O.A. Mokuolu, R.R. Olaosebikan, O.O. Folaranmi, M. Mayxay, M. Khanthavong, B. Hongvanthong, P.N. Newton, M.A. Onyamboko, C.I. Fanello, A.K. Tshefu, N. Mishra, N. Valecha, A.P. Phyo, F. Nosten, P. Yi, R. Tripura, S. Borrmann, M. Bashraheil, J. Peshu, M.A. Faiz, A. Ghose, M.A. Hossain, R. Samad, M.R. Rahman, M.M. Hasan, A. Islam, O. Miotto, R. Amato, B. MacInnis, J. Stalker, D.P. Kwiatkowski, Z. Bozdech, A. Jeeyapant, P.Y. Cheah, T. Sakulthaew, J. Chalk, B. Intharabut, K. Silamut,

S.J. Lee, B. Vihokhern, C. Kunasol, M. Imwong, J. Tarning, W.J. Taylor, S. Yeung, C.J. Woodrow, J.A. Flegg, D. Das, J. Smith, M. Venkatesan, C.V. Plowe, K. Stepniewska, P.J. Guerin, A.M. Dondorp, N.P. Day, N.J. White, Spread of Artemisinin Resistance in Plasmodium falciparum Malaria, N. Engl. J. Med., 371 (2014) 411-423.
[38] E. Moles, S. Galiano, A. Gomes, M. Quiliano, C. Teixeira, I. Aldana, P. Gomes, X. Fernàndez-Busquets, ImmunoPEGliposomes for the targeted delivery of novel lipophilic drugs to red blood cells in a falciparum malaria murine model, Biomaterials, 145 (2017) 178-191.
[39] E. Moles, P. Urbán, M.B. Jiménez-Díaz, S. Viera-Morilla, I. Angulo-Barturen, M.A. Busquets, X. Fernàndez-Busquets, Immunoliposome-mediated drug delivery to Plasmodium-infected and non-infected red blood cells as a dual therapeutic/prophylactic antimalarial strategy, J. Control. Release, 210 (2015) 217-229.
[40] J.M. Karle, R. Olmeda, L. Gerena, W.K. Milhous, Plasmodium falciparum: Role of Absolute Stereochemistry in the Antimalarial Activity of Synthetic Amino Alcohol Antimalarial Agents, Exp. Parasitol., 76 (1993) 345-351.
[41] F. Lehmann, Å. Pilotti, K. Luthman, Efficient large scale microwave assisted Mannich reactions using substituted acetophenones, Mol. Divers., 7 (2003) 145-152.
[42] R.E. Desjardins, C.J. Canfield, J.D. Haynes, J.D. Chulay, Quantitative assessment of antimalarial activity in vitro by a semiautomated microdilution technique, Antimicrob. Agents Chemother., 16 (1979) 710-718.
[43] M. Quiliano, A. Pabón, G. Ramirez-Calderon, C. Barea, E. Deharo, S. Galiano, I. Aldana, New hydrazine and hydrazide quinoxaline 1,4-di-N-oxide derivatives: In silico ADMET, antiplasmodial and antileishmanial activity, Bioorg. Med. Chem. Lett., 27 (2017) 1820-1825.
[44] J.D. Johnson, R.A. Dennull, L. Gerena, M. Lopez-Sanchez, N.E. Roncal, N.C. Waters, Assessment and Continued Validation of the Malaria SYBR Green I-Based Fluorescence Assay for Use in Malaria Drug Screening, Antimicrob. Agents Chemother., 51 (2007) 1926-1933.
[45] A. Daina, O. Michielin, V. Zoete, SwissADME: a free web tool to evaluate pharmacokinetics, drug-likeness and medicinal chemistry friendliness of small molecules, Sci. Rep., 7 (2017) 42717.
[46] I. Tetko, J. Gasteiger, R. Todeschini, A. Mauri, D. Livingstone, P. Ertl, V. Palyulin, E. Radchenko, N. Zefirov, A. Makarenko, V. Tanchuk, V. Prokopenko, Virtual Computational Chemistry Laboratory - Design and Description, J. Comput. Aided Mol. Des., 19 (2005) 453-463.
[47] Y. Oda, S.-i. Nakamura, I. Oki, T. Kato, H. Shinagawa, Evaluation of the new system (umu-test) for the detection of environmental mutagens and carcinogens, Mutat. Res.-Environ. Mutag. Related Subj., 147 (1985) 219-229.
[48] G. Reifferscheid, J. Heil, Y. Oda, R.K. Zahn, A microplate version of the SOS/umu-test for rapid detection of genotoxins and genotoxic potentials of environmental samples, Mutat. Res.-Environ. Mutag. Related Subj., 253 (1991) 215-222.
[49] W. Peters, The chemotherapy of rodent malaria, XXII. The value of drug-resistant strains of P. berghei in screening for blood schizontocidal activity, Ann. Trop. Med. Parasitol., 69 (1975) 155-171.

[50] W. Peters, B.L. Robinson, Chapter 92 - Malaria A2 - Zak, Oto, in: M.A. Sande (Ed.) Handbook of Animal Models of Infection, Academic Press, London, 1999, pp. 757-773.
[51] M.H. Arias, E. Deharo, A. Valentin, G. Garavito, Adaptation and optimization of a fluorescence-based assay for in vivo antimalarial drug screening, Parasitol. Res., 116 (2017) 1955-1962.
[52] G. Manzoni, S. Briquet, V. Risco-Castillo, C. Gaultier, S. Topçu, M.L. Ivănescu, J.-F. Franetich, B. Hoareau-Coudert, D. Mazier, O. Silvie, A rapid and robust selection procedure for generating drug-selectable marker-free recombinant malaria parasites, Sci. Rep., 4 (2014) 4760.
[53] O. Silvie, J.-F. Franetich, S. Charrin, M.S. Mueller, A. Siau, M. Bodescot, E. Rubinstein, L. Hannoun, Y. Charoenvit, C.H. Kocken, A.W. Thomas, G.-J. van Gemert, R.W. Sauerwein, M.J. Blackman, R.F. Anders, G. Pluschke, D. Mazier, A Role for Apical Membrane Antigen 1 during Invasion of Hepatocytes by Plasmodium falciparum Sporozoites, J. Biol. Chem., 279 (2004) 9490-9496.
[54] C.K. Wang, S.K. Weeratunga, C.M. Pacheco, A. Hofmann, DMAN: a Java tool for analysis of multi-well differential scanning fluorimetry experiments, Bioinformatics, 28 (2012) 439-440.
[55] R.C. MacDonald, R.I. MacDonald, B.P.M. Menco, K. Takeshita, N.K. Subbarao, L.-r. Hu, Small-volume extrusion apparatus for preparation of large, unilamellar vesicles, Biochim. Biophys. Acta, 1061 (1991) 297-303.
[56] E. Moles, K. Moll, J.-H. Ch'ng, P. Parini, M. Wahlgren, X. Fernàndez-Busquets, Development of drug-loaded immunoliposomes for the selective targeting and elimination of rosetting Plasmodium falciparum-infected red blood cells, J. Control. Release, 241 (2016) 57-67.
[57] C. Lambros, J.P. Vanderberg, Synchronization of Plasmodium falciparum erythrocytic stages in culture, J. Parasitol., 65 (1979) 418-420.
[58] A. Radfar, D. Méndez, C. Moneriz, M. Linares, P. Marín-García, A. Puyet, A. Diez, J.M. Bautista, Synchronous culture of Plasmodium falciparum at high parasitemia levels, Nat. Protoc., 4 (2009) 1899.
[59] K. De Klerck, D. Mangelings, Y. Vander Heyden, Supercritical fluid chromatography for the enantioseparation of pharmaceuticals, J. Pharm. Biomed. Anal., 69 (2012) 77-92.
[60] L.T. Taylor, Supercritical fluid chromatography for the 21st century, J. Supercrit. Fluids, 47 (2009) 566-573.

HIGHLIGHTS

- Nine aryl-substituted propanol derivatives (APD) show promising antimalarial activity.
- APD are active against chloroquine-sensitive and multidrug-resistant strains.
- The *in vivo* efficacy in the *P. berghei* mouse model shows compounds 66 and 72 to be promising candidates.
- Multistage activity profile (blood, liver, and mosquito stages).
- APD show unknown mechanism of action that differs from that of classical amino alcohols (e.g., hemozoin inhibition, plasmepsin II, and Hsp90).